COMPUTATIONAL MODELLING OF CARBON NANOTUBE REINFORCED POLYMER COMPOSITES

A THESIS SUBMITTED TO
THE BOARD OF CAMPUS GRADUATE PROGRAMS
OF MIDDLE EAST TECHNICAL UNIVERSITY
NORTHERN CYPRUS CAMPUS

BY

MUHAMMAD JIBRAN SHAHZAD ZUBERI

IN PARTIAL FULLFILLMENT OF THE REQUIREMENTS
FOR
THE DEGREE OF MASTER OF SCIENCE
IN
SUSTAINABLE ENVIRONMENT AND ENERGY SYSTEMS

JULY 2014

Approval of the Board of Graduate Programs

_____
Prof. Dr. M. Tanju Mehmetoğlu
Chairperson

I certify that this thesis satisfies all the requirements as a thesis for the degree of Master of Science.

_____
Assoc. Prof. Dr. Ali Muhtaroğlu
Program Coordinator

This is to certify that we have read this thesis and that in our opinion it is fully adequate, in scope and quality, as a thesis for the degree of Master of Science.

_____
Assist. Prof. Dr. Volkan Esat
Supervisor

Examining Committee Members

Assoc. Prof. Dr. Ali Muhtaroğlu	Electrical and Electronics Engineering Prog. METU NCC	_____
Assist. Prof. Dr. Volkan Esat	Mechanical Engineering Prog. METU NCC	_____
Assist. Prof. Dr. Behzat Kentel	Mechanical Engineering Prog. METU NCC	_____
Assist. Prof. Dr. Mustafa Erkut Özser	Chemistry Group METU NCC	_____
Assist. Prof. Dr. Ghulam Hussain	Mechanical Engineering Dept. Eastern Mediterranean U.	_____

I hereby declare that all information in this document has been obtained and presented in accordance with academic rules and ethical conduct. I also declare that, as required by these rules and conduct, I have fully cited and referenced all material and results that are not original to this work.

Name, Last name : Muhammad Jibran Shahzad, Zuberi

Signature :

ABSTRACT

COMPUTATIONAL MODELLING OF CARBON NANOTUBE REINFORCED POLYMER COMPOSITES

Zuberi, Muhammad Jibran Shahzad

M.S., Sustainable Environment and Energy Systems Program

Supervisor: Assist. Prof. Dr. Volkan Esat

July 2014, 92 Pages

This thesis investigates the effects of chirality and size of single-walled carbon nanotubes (SWNTs) on the mechanical properties of both SWNTs and carbon nanotube reinforced epoxy composites (CNTRPs). First, a novel 3D beam element finite element model is developed based on equivalent-continuum mechanics approach and used for replacing C-C chemical bond for modelling SWNTs. The effects of diameter and chirality on the Young's moduli, shear moduli, shear strains and Poisson's ratios of SWNTs are studied. For modelling CNTRPs, the aforementioned SWNTs are embedded into the epoxy resin finite element model. The volume fraction of SWNTs in epoxy is taken as 5% while the diameter for interface region between the two phases is taken twice to that of the SWNTs. For modelling interface regions, two approaches named as non-bonded interactions model and perfect bonding model are used and compared against each other. The latter approach is employed for evaluating the effects of chirality and size of SWNTs on the Young's modulus and Poisson's ratio of CNTRPs. The results for Young's moduli are in good agreement with those calculated by a theoretical relation known as continuum rule of mixtures. In order to quantify the structural mass reduction by using these CNTRPs for a particular application, specific strength is calculated for both pure epoxy resin and the composite. Result shows that the structural mass can be reduced 5 times compared to that of epoxy if its nanocomposite is used in its potential applications where the strength and volume requirements are fixed such as parts for automobiles and aircrafts. This mass reduction will ultimately lead towards better mileage, fuel savings and reduction in carbon emissions.

Keywords: SWNT, CNTRP, chiral effects, finite element model

ÖZ

KARBON NANOTÜP TAKVİYELİ POLİMER KOMPOZİTLERİN SAYISAL MODELLENMESİ

Zuberi, Muhammad Jibran Shahzad

Yüksek Lisans, Sürdürülebilir Çevreve Enerji Sistemleri Programı

TezYöneticisi: Yrd. Doç. Dr. Volkan Esat

Temmuz 2014, 92 sayfa

Bu tez Tek Duvarlı Karbon Nanotüpler'in (TDKNT) kiralite ve boyutlarının, Tek Duvarlı Karbon Nanotüpler (TDKNT) ve Karbon Nanotüp Takviyeli Epoksi Polimerler'in (KNTTP) mekanik özelliklerine etkilerini incelemektedir. İlk etapta, eşdeğer sürekli ortamlar mekaniği yaklaşımına dayalı üç boyutlu bir kiriş elemanı içeren yeni bir sonlu elemanlar modeli geliştirilmiş ve bu kiriş eleman karbon – karbon bağının modellenmesinde kullanılmıştır. TDKNT çapı ve kiralitesininYoung (elastisite) modülü, kesme modülü, kesme gerinimi ve Poisson oranı üzerine etkisi çalışılmıştır. KNTTP modellemesi için, geliştirilen TDKNT sonlu elemanlar modeli epoksi reçine matris sonlu elemalar modeline entegre edilmiştir. Kompozit içindeki karbon nanotüp oranı hacmen %5 alınmış, karbon nanotüp – epoksi matris arasındaki arayüzey bölgesinin çapı karbon nanotüp yarıçapının iki katı olarak kabul edilmiştir. Arayüzey bölgesinin modellenmesi için bağsız etkileşimler modeli ve mükemmel bağ modeli adı verilen iki yaklaşım kullanılmıştır. Mükemmel bağ modeli kullanılarak, TDKNT'lerin kiralite ve boyutlarının KNTTP'lerinYoung (elastisite) modülü ve Poisson oranı üzerine etkisi değerlendirilmiştir. Elde edilen Young (elastisite) modülü sonuçları, sürekli ortamlar karışımlar kuralı kullanılarak elde edilen teorik sonuçlara oldukça yakındır. KNTTP'leri içeren belirli bir uygulama için kütlesel azalmayı belirlemek amacıyla epoksi reçine ve kompozit için öz mukavemet değerleri hesaplanmıştır. Sonuçlar çeşitli otomotiv ve uçak parçalarında kompozit kullanımının sadece epoksi reçine kullanımına kıyasla kütlede 5 kata varan azalmayı mukavemetsel kayıp olmaksızın sağladığını göstermiştir. Bu kazanımlar çeşitli taşıtlar için az yakıtla daha uzun mesafe alınmasını ve karbon salınımın azalmasını sağlayacaktır.

Anahtar Kelimeler: Tek duvarlı karbon nanotüp (TDKNT), Karbon nanotüp takviyeli polimer (KNTTP), kiralite etkileri, sonlu elemanlar modeli

DEDICATION

To my beloved

"NAGHMA KHALA (Late)"

And also to my

"GRANDPARENTS, PARENTS AND SISTER YOUSRA"

ACKNOWLEDGEMENTS

I would like to express my deepest gratitude to my advisor Dr. Volkan Esat for his continuous support, advice and guidance throughout my research. I would like to thank him for supporting me through the difficult times of not only my master's degree but also my personal issues during this period. I would also like to thank him for tolerating the delays from my side during the course of this work.

Besides my advisor, I would also like to thank the other members of my jury, Dr. Ali Muhtaroğlu, Dr. Behzat Kentel, Dr. Mustafa Erkut Özser and Dr. Ghulam Hussain, for their encouragement, insightful comments, and suggestions throughout the research and reviewing process.

I would also like to express my sincere gratitude to METU-NCC and Chemical Engineering Program Co-ordinator Prof. Dr. Türker Gürkan for providing me with an assistantship which helped me immensely in funding my masters and stay in Northern Cyprus. I would also like to pay my kindest regards to all the faculty members of Chemical Engineering Program for their kind support.

I would like to acknowledge my friends and colleagues who helped me in my work. I would like to thank Abdullah Mohiuddin Siddiqui and Syed Muhammad Hasan Ali for their fruitful inputs and discussions regarding the research. Beside the technical help and support, I really appreciate the efforts made by Muhammad Azhar Ali Khan, Syed Zaid Hasany, Muhammad Arsalan Tariq, Fassahat Ullah Qureshi, Rayaan Harb, Furkan Ercan, Moslem Yousefzadeh, Sajed Sadati, Musa Hadera, Kumudu Gamage and many others helping me in having a good time on the campus.

At last but definitely not the least, I would like to express my love, affection and kindest regards to my father Mr Muhammad Shahzad Zuberi and mother Mrs Saba Shahzad in particular and relatives in general for their continuous prayers and support. This would not have been possible without them.

Muhammad Jibran Shahzad Zuberi

TABLE OF CONTENTS

LIST OF TABLES

LIST OF FIGURES

NOMENCLATURE

2α	Change in rotational angle (rad)
$\emptyset$	Torsional angle (rad)
γ	Shear strain
ε, σ	Lennard-Jones parameters (kJ/mol)
ν	Poisson's ratio
A	Area (nm^2)
a	Length of unit vector (nm)
C	Circumference (nm)
C_h	Chiral Vector written as a coordinate *(n, m)*
C_{wt}	Thickness constant (TPa/nm)
d	Diameter (nm)
E	Young's Modulus (TPa, GPa)
F	Force (nN)
G	Shear Modulus (TPa, GPa)
I	Moment of inertia
J	Polar moment of inertia (nm^4)
k	Force constant (nN/nm for bond stretching, (nN nm)/rad^2 for bond angle variation and torsional stiffness)
L	Length (nm)
R	Radius of representative volume element (nm)
r	Radius, Intermolecular distance (nm)
T	Torsional load (nN nm)
t	Thickness (nm)
Vf	Volume fraction (%)
V	Steric Potential Energy
W	Width (nm)
$\Delta\theta$	In-plane increment (rad)
$\Delta\varphi$	Twisting angle increment (rad)
$\Delta\beta$	End beam rotation (rad)
ΔL	Change in length (nm)
Δr	Bond stretching variation (nm)

Subscripts

θ	Bond angle variation
φ	Dihedral angle
τ	Combined energy due to dihedral angle and out-of-plane torsion
ω	Out-of-plane torsion
c	Composite
cnt	Carbon nanotube
g	Graphene sheet
m	Polymer matrix
o	Initial measurement
r	Bond stretching
RVE	Representative volume element
t	Total steric potential energy
vdw	Van der Waals

Chapter 1

INTRODUCTION

A severe damage to the ecology and environmental balance of the planet has been realised worldwide due to the rapid growth in industrialisation. It is a mutual conscience that the technology in future will need to incorporate concepts like minimum energy consumption, biological sustainability and sustainable raw materials. Modern research and development (R&D) needs development of high value and safer products. Advanced composite materials such as nanocomposites are observed to have advantages when compared to conventional materials in several areas, predominantly in low energy usage during fabrication, construction and subsequent assembly operation. The sustainability assessment of the final products is of supreme importance right from the initial stage of synthesis to the final stage of disposal. This assessment comprises of green synthesis, processing, recycling, applications and biodegradation. In spite of having environmental issues associated with the material fabrication, principally resins, numerous manufacturers are already improving this characteristic drastically [1].

Researchers in both industry and academia are taking a keen interest in developing advanced nanocomposites with multifunctional features. Carbon nanotubes (CNTs) are unique nanostructured materials which possess extraordinary physical and mechanical properties. It is their remarkable properties that bring interest in using CNTs as filler in polymeric matrix to get ultra-light structural materials and referred to as carbon nanotube reinforced polymer composites (CNTRPs) [2]. Polymer composites are manufactured for a number of commercial applications including sports goods, automobile parts, aerospace components, health and medicine, electronics and computing, energy, environmental transportation etc. One major obstacle to the use of nanocomposites commercially is the lack of comprehensive structure-property relationships and effective processing techniques. It is essential to have multi-layered structured composites in which each sub-layer serves an individual purpose to yield a mechanically integrated and multifunctional material [1].

A strong emphasis has been noticed in the past 20 years for the development of polymeric nanocomposites where one of the dimensions of the filler is of nano-metric order. A robust growth in computer technology has enabled researchers to characterise and simulate the properties of these composites at the nanoscale via modelling and simulations. The unique blend of nanocomposites' characteristics such as mechanical and surface properties, size, and level of concentration essential to bring change in a polymer matrix, tied with advance simulation techniques have attracted great interest in this area.

1.1. Background

A CNT is a hexagonal network of carbon atoms rolled into hollow, seamless cylinder often capped with half of a fullerene molecule at each of its ends. In spite of having similarity in chemical composition between CNTs and graphite, CNTs are highly isotropic; a property that differentiates CNTs from other forms of carbon structures. CNTs are classified into two types: Single-walled carbon nanotubes (SWNTs) having discrete cylinders of approximately 1-2 nm diameter; and multi–walled carbon nanotubes (MWNTs) made up of several concentric cylinders bound together by weak van der Waals forces. Both types are shown in Figure 1.1. It is the diameter, chirality and type of the nanotube that defines its properties [2].

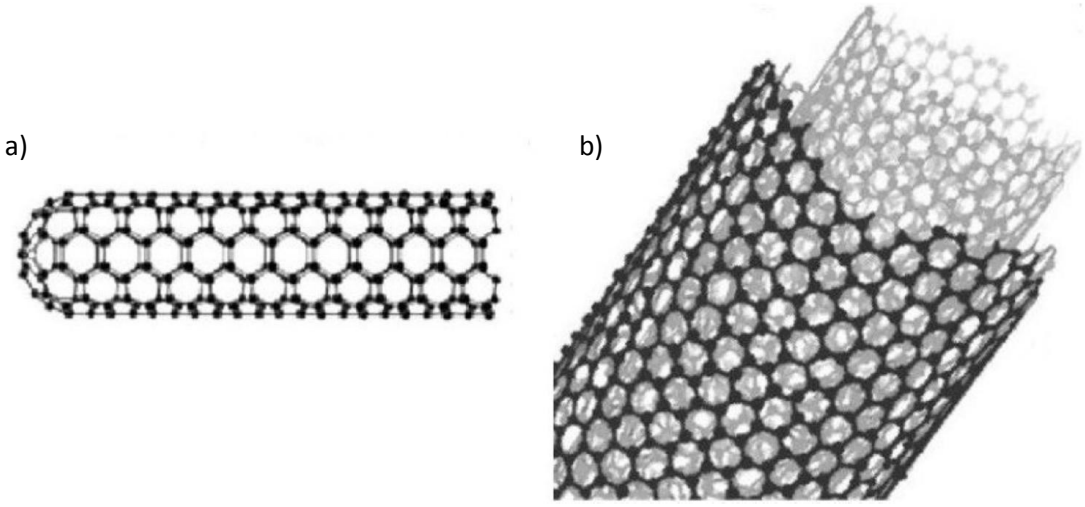

Figure 1.1 a) Single-walled nanotube, b) Multi-walled nanotube [2]

Physical properties change dramatically by the transition of particles from micro to nano scale. Nanomaterials have comparatively large surface area for a fixed volume which results into

different properties from the larger-dimensional material (macromolecules with less surface area) of the same composition. Surface area per unit volume for particles and fibres is inversely proportional to the diameter of the material. Therefore, smaller the diameters as in case of nanotubes, greater the surface area per unit volume. Figure 1.2 shows common particle geometries and their respective surface area to volume ratios. Surface area to volume ratio is dominant for fibrous and layered nanomaterials, by the first term in the equation demonstrated in Figure 1.2. The second term is often omitted as it is negligible compared to the first term. Carbon nanotubes are characterized as fibrous materials [3].

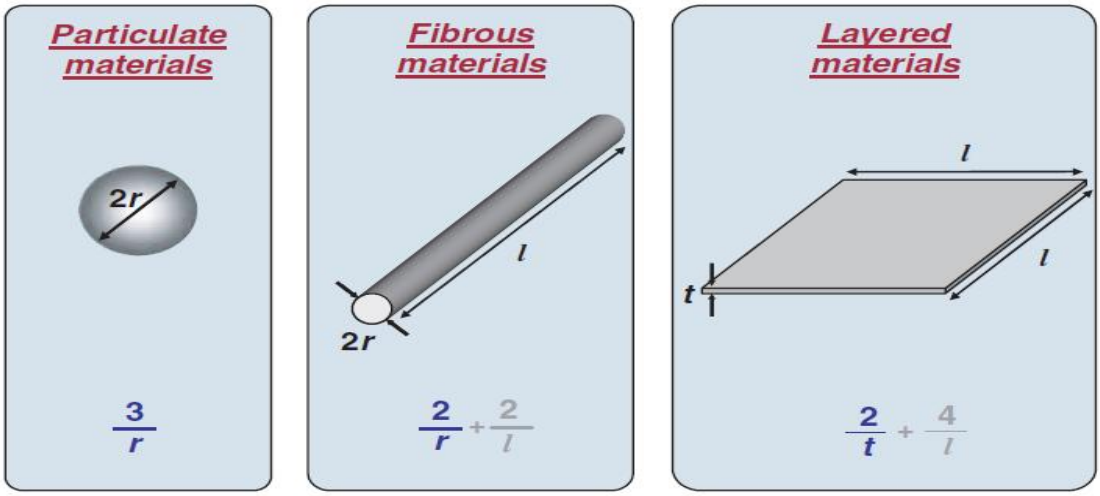

Figure 1.2 Common particle reinforcements/geometries and their respective surface area-to-volume ratios [3]

In fibre reinforced polymer composites such as CNTRPs, adequate dispersion of fibrous material into polymer matrix and its adhesion at the fiber-matrix interface play a critical role in determining the mechanical properties of the nanocomposite material. Poor dispersion may degrade the mechanical properties. Also, by improving interfacial bond between the fibre and the polymer matrix, one can alter the properties of the composite. For example, good interfacial adhesion will optimise properties like inter-laminar shear strength, delamination resistance, corrosion resistance and fatigue. Some of the most commonly used fabrication methods for nanostructured polymer composites are Resin Transfer Molding (RTM), Vacuum Assisted Resin Transfer Molding (VARTM), Wet lay-up, Pultrusion, Resin Film Infusion (RFI), Filament Winding, and Fibre Placement Technology [3].

1.2. Geometric Structure of CNTs

As stated earlier, CNTs are the seamless and rolled-up graphene sheet with constant radius comprising of hexagonal network of carbon atoms. This benzene type hexagonal set-up recurs periodically as each carbon atom is bonded strongly by covalent linkages to the three adjacent atoms. These covalent bonds play a substantial role to the outstanding mechanical properties of graphene and CNTs [4]. The atomic structure of CNTs depends upon its chirality unique to each and every nanotube. Chirality of CNTs is defined by the packing of carbon hexagons in the graphene sheets and represented by a chiral vector *(n, m)* and chiral angle. The indices of the chiral vectors indicate the morphology of CNTs and change in morphology alters the nanotube properties [5]. The geometric representatives are plotted in Figure 1.3.

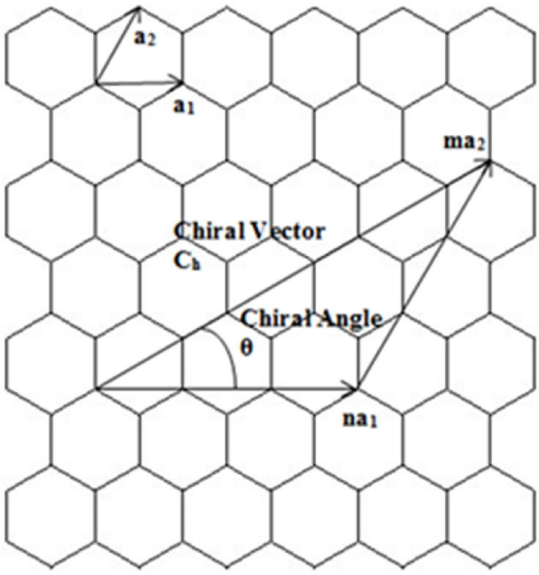

Figure 1.3 Schematics of hexagonal network of graphene sheet displaying structural parameters

The chiral vector is defined as [5]:

$$\boldsymbol{C_h} = n\boldsymbol{a_1} + m\boldsymbol{a_2} \tag{1.1}$$

where 'a_1' and 'a_2' represents the unit cell base vectors of the graphene sheet. *'a'* is the length of unit vector defined as:

$$a = \sqrt{3}L \tag{1.2}$$

where 'L' is the bond length taken as 0.142 nm. The circumference 'C', the diameter 'd' and the chiral angle 'θ' of the SWNTs is defined as [4]:

$$C = a\sqrt{n^2 + nm + m^2} \tag{1.3}$$

$$d = \frac{C}{\pi} \tag{1.4}$$

$$\Theta = sin^{-1}\frac{\sqrt{3}m}{2\sqrt{n^2 + nm + m^2}} \tag{1.5}$$

Based on Equations 1.1-1.5, there are following three classifications of CNT structures, shown in Figure 1.4 as well;

a) armchair *(n, n)*
b) zigzag *(n, 0)* and
c) chiral *(n, m)*.

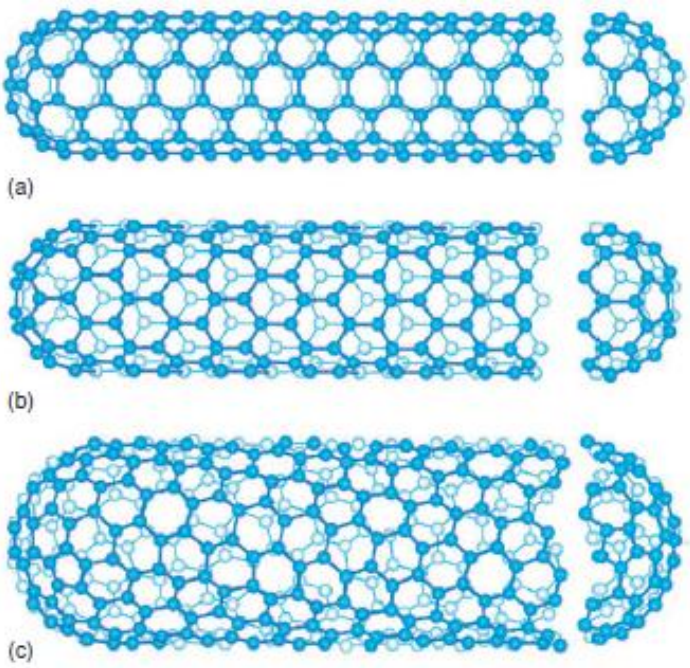

Figure 1.4 Schematic of nanotube morphologies a) armchair, b) zigzag, c) chiral [3]

where *'n'* is greater than *'m'* and are not equal to each other. The chiral angles of the zigzag and armchair structures are 0^o and 30^o, respectively, while for chiral structure, the angle varies between 0^o and 30^o. If *'(m – n)/3'* gives an integer, the resulting structure is metallic otherwise it is semi-conducting. All armchair and one-third of the zigzag nanotubes have continuous conduction band which leads them to a metallic structure while the remaining two-third of the zigzag nanotubes are semiconductors having an energy gap in the conduction band [3], [6].

1.3. Mechanical Properties of CNTs

Tensile and compressive strengths are defined as the maximum tensile and compressive loads respectively a material can bear before failure. Both tensile and compressive strengths of CNTs are twice higher than the current high-strength carbon fibres known in magnitude. Their density is lower, i.e., 1.3 g/cm^3, approximately when compared to the commercial carbon fibres (1.8-1.9 g/cm^3). Improvement in material strength implies the replacement of commercial carbon fibres with CNTs reducing weight and size of the structural composite parts significantly which will lead towards sustainable development. Young's modulus is the measure of stiffness of an elastic and isotropic material. In comparison with carbon fibres (Young's Modulus 750 GPa) [2], [4], CNTs have a higher modulus ranging between 1-5 TPa and crowned as the stiffest material ever made [7]. Figure 1.5 compares the tensile strength of CNTs with some of the other conventional materials and demonstrates its great ability to withstand high impacts and stresses. The most notable effect is the combination of high strength with stiffness and flexibility which is lacking in carbon fibres. Carbon nanotubes as mechanical springs would be very stiff for minor loads but for larger loads would turn soft yielding large deformations without breaking [2].

CNTs can be twisted, flattened and buckled when deformed reversibly. High value of strain in a material at the point of fracture shows the maximum stress a material can bear before failure. Fracture strains of CNTs lie between 10% - 30%, greater than most carbon fibers (0.1% - 2%) which means CNTs have a greater ability to withstand large stresses before breaking. Aspect ratios of CNTs can reach up to 10,000 which add benefit for imparting strength to composite systems. The excellent mechanical properties of CNTs encourage their use as reinforced fibres in high-toughness nanocomposites such as CNTRPs, where strength, stiffness and low weight characteristics are required [2].

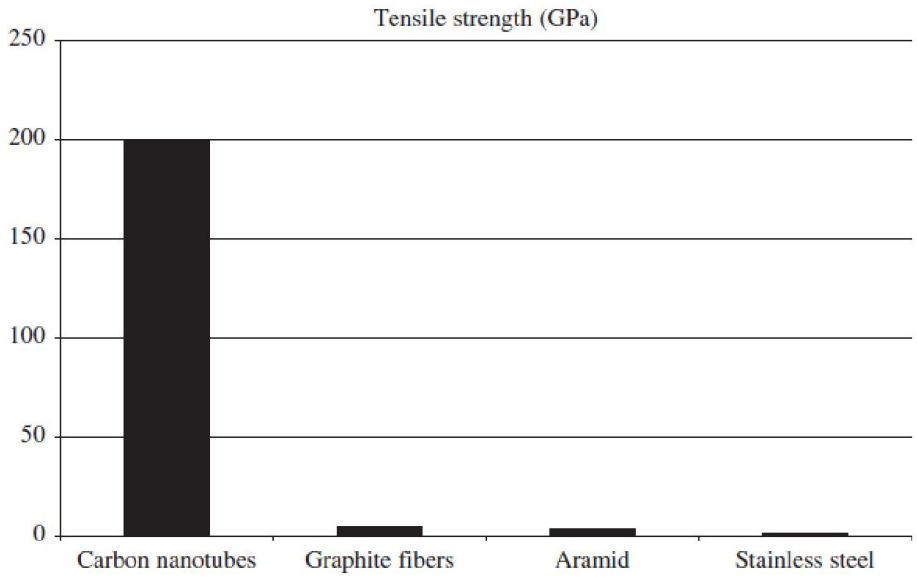

Figure 1.5 Comparison of tensile strength of common engineering materials [3]

1.4. CNT Orientation and Dispersion into Polymer Matrix

Orientation in the direction of applied forces permits greater load transfer. Orientation other than the direction of the applied force may not show the full potential of the nanotube. Additionally, nanotubes oriented in the same direction allow easier transfer of either thermal or electrical energy. Also, dispersing SWNTs and higher concentrations of MWNTs into a polymer matrix is a difficult task to perform due to their accretion as a result of van der Waals attractions between the nanotubes. SWNTs form ropes or bundles more easily as compared to MWNTs due to their size; therefore, producing SWNTs require more specialisation than MWNTs and more cost of purification. Most of the composite researchers consider SWNTs as ultimate reinforcements for the next generation high performance composite materials. On the other hand, MWNTs possess relatively low values for its mechanical, thermal and electrical properties as compared to SWNTs due to the fact that these concentric nanotubes slide past each other. Also, MWNTs tends to have a larger diameter to the magnitude of 10 times more than SWNTs due to their geometry, i.e., inherent tube within a tube structure. However, improvements have been made to produce MWNTs with smaller and precise diameters [8].

1.5. CNTRPs as Sustainable Materials

Polymer nanocomposites are anticipated to encompass in every aspect of life in the mid and longer term, similar to the fashion plastics did in the past century. There is an incredible technological and economic potential associated with CNTRPs which need to be explored. CNTs usually do not break down as a result of subsequent processing. Therefore, recycling is possible without compromising its unique properties. They have an advantage of recycling thermoplastic composites which not only improve cost effectiveness but also contribute towards environmentally benign advanced nanotube materials. CNTs can be added during compounding without the mechanical and processing properties of the polymer matrix being compromised. As a result, the finished product is light in weight, tempting in surface finish, resistant to corrosion and less expensive to ship. CNTRPs offer more security during transportation and handling as it is less susceptible to dents, scratches and chips. Also, C-C bonds are one of the strongest in nature and a structure grounded on a perfect arrangement of bonds oriented along the axis of CNTs gives birth to a very strong material with extremely large strength-to-weight ratios [2].

There is a diverse range of applications where CNTRPs have proved themselves as an attractive switch from conventional materials. Donnell et al. [9] studied the impact of CNTRP on the performance of four airframes. Flight profiles of CNTRP with 70% SWNT by volume in the polymer matrix were modelled by utilizing Euro Control's Base of Aircraft Data (BADA) and traditional flight dynamics theory, and fuel consumption was evaluated by constructing flights from take-off to landing. Reduction of 14.05% on average in structural mass was observed by replacing aluminium airframes from CNTRP-structured airframes. 9.8% fuel on average was saved and flight range increased to 13.2% on average. Enhanced Traffic Management Systems (ETMS) empowered a correlation of fuel consumption savings to actual fuel savings for some of the common flight paths for the aircraft types under investigation.

Automobile bumpers is another application of CNTRPs as these bumpers will have good mechanical properties and are lighter in weight when compared to the standard fibre-glass bumpers (only 1-5 wt% will be needed compared to 30% or more of fibre-glass). Use of CNTRPs can be encouraged for automobile bumpers due to their multi-functionality, good mechanical properties, light weight and electrical conductivity. The conductivity will permit direct application of electrostatic spray of base and clear coats, due to which the need for an additional primer coat prior to painting will be eliminated. Other advantages include saving

paint consumption and reducing volatile emissions from paint lines. Electrostatic painting may also be extended to door handles, mirror shells and grills. In order to increase conductivity for electrostatic painting, Hyperion Catalysis International Inc. manufactured plastic side view mirror housings for Ford Taurus [2].

Cheap, renewable energy sources are the driving force for the research being carried out extensively on photovoltaic technologies. Hence, CNTRPs have an important application in organic solar cells as well. There are several other examples available in literature that substantiates the contribution of CNTRPs towards sustainable development.

1.6. Epoxy Resin and its Sustainable Aspects

Although there is a huge debate on the sustainable use of polymers since other than their remarkable and unique properties, they also contribute a lot towards waste generation. They are flexible yet sometimes low in strength. Curing is a process of introducing crosslinks between the polymeric chains with the help of curing agents to get higher strength of polymers but once cured, these polymers cannot be recycled. Another issue associated with the polymers is that they are non-biodegradable and can stay in their original form for years. It is due to the risks involved with the polymers degrading environment, researchers in material science have started to improve the performance of these polymers by adding additives for either biodegradation or performance enhancement which ultimately leads towards a larger life span of the material and CNTs are added to serve the later purpose resulting into CNTRPs.

CNTRPs consist of a polymer matrix at the outer surface which receives the load and transfers it to the SWNTs embedded into it. From the modelling point of view, this polymer matrix has to be assigned material properties for the simulations. Therefore, epoxy resin is selected to be the matrix around SWNTs due to several reasons from the sustainable point of view discussed later in this section. Epoxy resins are those having more than one epoxy group capable of being transformed into a polymeric chain upon polymerization process. This epoxy group is often referred to as oxirane group containing an oxygen atom bonded with carbon atoms which are further bound by separate atoms. Epoxy resins have a wide range of applications such as adhesives, construction materials, laminates, and coatings, textile finishing and automobile parts. Dry epoxy resin systems are used in aircraft construction and find applications in marine

industry by replacing polyesters in special applications where underwater strength is important [10].

Level of adhesion is one of the most important considerations while selecting polymer matrix for the CNT reinforcement. Epoxy resins form strong bonds with almost all surfaces except a few nonpolar substrates which make them suitable for CNT dispersion with higher adhesion. Other than the outstanding properties of the epoxy resins, they have several sustainable aspects associated with it which encourages their usage for the fabrication of nanocomposites for high-tech applications. On curing, epoxies do not cause volatile emissions in spite of the presence of volatile solvent into it. Epoxy resins are also used to form lightweight structures with good insulation properties which is one of the notable aspects of epoxies from the sustainable point of view [10]. Reducing weight of composite by specialised design improves environmental management by reducing material consumption that ultimately be landfilled or recycled. Technology for recovering epoxy resin from its nanotube composites for reuse is in its premature stage. Studies suggest that recovery is achievable through gasification and a few more processes. As stated earlier, CNTs can be extracted from the composites completes its lifetime to be used in a different application with lower requirement of its mechanical properties. Therefore, recovery of both phases from their composites is a huge value addition towards sustainable development.

1.7. Research Opportunities

Based on the literature review presented in Chapter 2 identifies the following research questions in general to be addressed for improved mechanical properties of CNTRPs:

i. How can the adhesion between CNT and polymer matrices be improved?
ii. What should be the manufacturing technology to have good CNT dispersion into the polymer matrix?
iii. How do the properties of CNTRPs change by adding CNTs into matrix in different ratios?
iv. What are the effects of chirality and size of CNTs on the mechanical properties of CNTRPs?
v. What are the sustainable aspects of CNTRPs?

There are several other questions that exist under each aforementioned research umbrella. For example, there is a debate on which technology should be used to achieve higher efficiency of CNT dispersion into the polymer matrix. Contrary to that use a common solvent which not only dissolves polymer resin but also allows efficient dispersion of CNTs as well without changing the technology [11], [12].

1.8. Thesis Overview

Several works should be deeply investigated to enhance the mechanical properties of advance composite materials like CNTRPs. This is a challenging yet interesting area for the people working in the composites community. As the prime objective is to improve the mechanical properties of CNTRPs, various aspects of it should be inspected thoroughly to achieve the goal. Presently, there are very few reports and papers available in the literature that explains the effect of CNT chirality, chiral angle and its diameter on the properties of CNTRPs. This thesis proceeds with the aim to examine the effect of chirality and diameter of SWNTs on the mechanical properties of CNTRPs computationally so that their performance in their potential applications is encouraged which will not only save material, energy and costs but also serve as a building block towards sustainability. In other words this thesis is dedicated to answer Question iv of Section 1.7 in particular and Question v in general.

Chapter 2

LITERATURE REVIEW

Material science is presently undergoing a shift from developing traditional materials to developing nanostructured materials as they are functionalised, self-assisting and sometimes self-healing [2]. Field of conventional composite materials can be redefined by the nanocomposites both in terms of performance and applications. Polymer nanocomposites hold the potential to replace current composites and create new markets. Carbon nanotube reinforced polymer composites (CNTRPs) are highly promising composite materials possessing the potential to be used in various areas such as automotive, aerospace, defence, and energy sectors. Although they are utilised in various important and appealing applications, CNTRPs still need major breakthroughs.

One important issue involving most of the CNT/polymer nanocomposites is to determine whether the unique properties of polymers can be ascribed to the large aspect ratios and small dimensions of CNTs. Another issue is to determine whether the surface area of CNTs promotes interactions adequate for load transfer between the phases. Also, it is important to investigate how chemical bonds between CNT and matrix can improve the shear strength of the nanocomposite [2]. Han et al. [13] studied the defective structures and properties of nanotubes by generating model configurations. They found that MWNTs had more defects as compared to SWNTs which were relatively defect free. Nanotubes are functionalised to improve their dispersion and compatibility in the polymer matrix but there exists a few concerns like whether the properties of the final product will improve by functionalisation of a nanotube [3].

One of the biggest challenges is developing the fabrication technology in terms of value for commercialisation and quality. For example, efficient dispersion of nanotubes into the polymer matrix and the chemical compatibility between the two is a critical issue. Surface properties of CNTs affect their dispersion within a polymer matrix and by using traditional compounding methods, it is difficult to disperse nanotubes homogenously in a polymer matrix due to the tendency of nanotubes to accumulate and form bundles due to van der Waals forces between the nanotubes. These agglomerated nanotubes commonly split when subjected to force at the same time causing a premature failure in the final product [3], [8].

Several works have been done to address the aforementioned issues in general. This chapter presents the literature review done to identify the research questions regarding applicability of CNTRPs.

2.1. Gap in Literature

Varied experimental and simulation results on the mechanical properties of CNTRPs have been reported by various researchers and scientists since its emergence. Some of which are discussed following to explain the necessity of further research in this highly competitive area.

Elastic modulus represents the stiffness of a material in the elastic range, which can also be defined as resistance to elastic deformation. Elastic modulus is referred to as Young's modulus when axial load is applied to the material while as shear modulus under torsional load application. When unparalleled high elastic modulus and tensile strength of CNTs integrate into a polymer matrix, it does not always ensure enhancement in mechanical properties of a composite. Both encouraging and discouraging results have been seen in the past. In some studies, mechanical properties even degraded when CNTs were added to a polymer matrix. Bhattacharya et al. [14] investigated melt blended composite of SWNT/PP (polypropylene) and observed a minute drop in elastic modulus, tensile strength and fracture strain with 0.8 wt.% CNT addition. Flexural strength is the ability of a material to resist deformation when bending load is assigned to it. In another research conducted by Lau and Shi [15], flexural strength of CNT/epoxy composite failed to increase with 2 wt.% CNT addition. Jia et al. [16] determined that tensile strength, hardness and toughness of the CNT/PMMA (poly methyl methacrylate) composite decreases with untreated CNT.

Some studies exhibit slight increase in elastic modulus with almost no increase in mechanical strength of CNTRPs. Schadler et al. [17] presented in their study that the tensile modulus of CNT/epoxy composite was improved by about 20% while 24% improvement was made in the compressive modulus by adding 5 wt.% of CNT into the polymer matrix. Yield strength of a material is the value of stress at which plastic deformation starts to occur. In a study by Haggenmueller et al. [18] on aligned SWNT/PMMA composite, elastic modulus and yield strength were reported to increase moderately with an increase in draw ratio and nanotube loading. Wong et al. [19] studied MWNT/PS (polystyrene) rod samples from an extrusion

process. They observed that tensile stiffness was increased by approximately 10% and tensile strength was also somewhat improved.

In some cases, the mechanical properties were improved significantly by the reinforcement of CNTs into polymer matrices. In a study by Qian et al. [20] showed that both elastic modulus and tensile strength of MWNT/PS composite was increased by 36-40% and 25% respectively after adding 1 wt.% CNT into the matrix. Liu et al. [21] compared the elastic modulus and yield strength of neat PA6 (nylon-6) and MWNT/PA6 composite and their results showed that by incorporating only 2 wt.% MWNT, modulus and strength enhanced by about 214% and 162% respectively for the composite. Ganguli et al. [22] demonstrated that with the addition of 1 wt.% of MWNT in the polymer matrix of a bi-functional epoxy resin, ultimate strength and strain to failure improved up to 139% and 158% respectively.

In parallel with some of the experimental results shown above, simulation results over such systems also demonstrate diversified conclusions which create opportunities for scholars to investigate CNTRPs more until outcomes of the different studies start to converge. A detailed literature review for modelling CNTs and CNTRPs addressing their mechanical properties is presented in the next two sections.

2.2. Literature Review for Modelling SWNTs

Most of the researchers consider single-walled carbon nanotubes (SWNTs) as ultimate reinforcements for the next generation high performance composite materials. On the other hand, multi-walled carbon nanotubes (MWNTs) possess lower mechanical, thermal and electrical properties due to the fact that these concentric nanotubes slide past each other as stated earlier [3]. Hence, the present study is mainly focused on SWNTs.

A number of experimental studies have been carried out to estimate the mechanical properties of CNTs and the methods to measure these mechanical properties are primarily based on atomic force microscopy (AFM) and transmission electron microscopy (TEM) [4]. Literature review of this particular study and few others suggests that there exists a great erraticism among these experimental results due to the complexities associated with the characterisation on nano-scale. Also, there is paucity in the literature on the effects of size and chirality on the mechanical properties of CNTs. Insight into the aforementioned issues may be gained through computational techniques time- and cost-effectively as compared to experimentation.

Computational modelling of CNTs for the assessment of their mechanical properties is thought to be a powerful tool when compared to the experimental handicaps [4].

The computational approaches can be classified into molecular mechanics including ab initio and classical molecular dynamics (MD) approaches and continuum mechanics approach [23]. The results determined from ab initio methods are relatively more accurate as compared to MD methods but at the meantime, they are computationally expensive and effective for small systems involving a few hundreds of carbon atoms. It is due to this fact that MD methods have been applied comprehensively for CNTs' material characterisation as these methods can be used for large systems simulating millions of atoms ranging from 10^6 to 10^8 on a shorter time span less than 10^{-6} to 10^{-9} seconds. Methods involving continuum mechanics approach are capable of simulating large systems with longer time scale as these systems are modelled as continuum medium rather than discrete particles [4], [23]. Continuum mechanics is an essential way of studying nonlinear behavior of materials. Among the nonlinear phenomena that can be introduced are chaotic dynamics, instabilities and complexity. Another advantage of continuum mechanics is its potential to demonstrate the phenomena of fracture and failure of solids which is difficult to model [24]. One of the leading developments in continuum methods recently is the 'Equivalent-continuum model (ECM)' approach. ECM syndicates molecular mechanics (MM) and finite element method (FEM) together which is now considered an efficient technique particularly for nanostructures with large scale.

Equivalent-Continuum Mechanics method primarily implicates continuum shell, continuum truss and continuum beam modelling [4]. Yakobson et al. [25] studied the behavior of CNTs beyond Hooke's law by a continuum shell model and reported 5.5 TPa as the Young's modulus of nanotube. Natsuki and Endo [26] developed a study using continuum shell modelling to evaluate the elastic moduli of a zigzag and an armchair nanotube and found a value of 0.94 TPa. Pantano et al. [27] also conducted a research based on continuum shell modelling and found the Young's modulus of CNTs to be 4.84 TPa. As CNTs are simulated with shells in this approach, it neglects their atomic characteristics, hence in that way any possible effect that may influence the mechanical behavior of CNTs is eliminated. Another limitation associated with continuum shell modelling is that it does not consider interatomic forces [4].

Odegard et al. [28] developed a continuum truss model and established a relationship between effective bending rigidity and molecular properties of a graphene sheet by comparing the

molecular potential energy of CNTs with the mechanical strain energy. Meo and Rossi [29] used the same method and predicted the ultimate strength and strain of SWNTs along with the effects of chirality and deflections on it. Their results demonstrated the Young's modulus of 0.920 TPa for armchair structures and 0.912 TPa for zigzag structures. Continuum truss models fail to take C-C bond inversion and bending into account. Therefore in studies where the effects of local bending and out of plane deformations are significant, truss models cannot be used [4].

Li and Chou [30] developed a continuum beam model by replacing C-C bonds with beam elements. They determined the elastic moduli of these beam elements by linking molecular and continuum mechanics together. They assumed the cross section of the beam elements to be circular and found the Young's modulus for armchair and zigzag CNTs to be in between 0.995 TPa to 1.033 TPa while the shear modulus to be in the range of 0.250 TPa and 0.485 TPa. Xiao et al. [23] developed a finite element beam model by incorporating modified Morse potential and evaluated Young's modulus, shear modulus, Poisson's ratio and stress-strain relationships for armchair and zigzag SWNTs only under both axial and torsional loading conditions. Their results indicated the Young's modulus to be in the range of 1 to 1.2 TPa, shear modulus from 0.40 to 0.45 TPa and Poisson's ratio as approximately 0.2.

Tserpes and Papanikos [31] evaluated both Young's and shear modulus of SWNTs by finite element modelling using the similar approach developed by Li and Chou [30]. They studied the influence of chirality on the elastic moduli of SWNTs and reported a Young's modulus of 2.337 TPa for armchair nanotube (8,8). Jalalahmadi and Naghdabadi [32] utilized FEM and Morse potential to find the mechanical properties of the beam elements, and determined that Young's modulus ranged from 3.296 to 3.514 TPa. Recently, Lu and Hu [4] have simulated C-C bond with the cross sectional area being elliptical. They obtained the Young's modulus of SWNTs to be 0.989 TPa to 1.058 TPa and Shear Modulus to be 0.237 TPa to 0.469 TPa. In this thesis equivalent-continuum beam modelling approach is used to model SWNTs as it takes into account more factors and parameters which shell and truss models are incapable to incorporate in.

2.3. Literature Review for Modelling CNTRPs

Although there is large scatter of values in literature regarding the mechanical properties of SWNTs but at least similar studies can be found applying different approaches and techniques

for several aims and objectives. When it comes to model CNTRPs by embedding developed SWNTs into the polymer matrix, very few studies are found in literature on the subject which creates a great opportunity to work in this direction. Ayatollahi et al. [33] proposed a multi-scale representative volume element (RVE) representing CNTRP for finding the mechanical behaviour under tensile, bending and torsional loading of the nanocomposites. They found the effect of interface stiffness on tensile, bending and torsional properties on two RVE configurations. The stiffness of the RVE was found to be affected much more by a strong interface than by a weaker interface with a low value of Young's modulus. Furthermore, the stiffness of the nanocomposite was found to be most affected by the stiffness of the interface under bending loading conditions.

In order to study the effect of CNT on fracture properties of the polymer composite, Rafiee et al. [34] constructed a 3D finite element model of single-walled carbon nanotube reinforced polymer. The RVE took into account the lattice structure of CNTs and simulated the surrounding polymer using solid elements. They used van der Waals interactions for load transfer from the host polymer matrix to the CNT. In the next step they replaced CNT and interface region by perfectly bonded solid fiber with Young's modulus of 1 TPa for investigating the importance of lattice structure of CNT and non-bonded interface region in modelling process. They concluded by claiming non-bonded interface region being a better approach for reinforcement against crack propagation.

Rafiee and Moghadam [35] investigated the impact and post-impact behavior of a CNTRP based on cylindrical representative volume element (RVE) consisting SWNT dispersed into a polymer matrix. A 3-D beam element was used to model each C-C bond in the CNT lattice structure. CNT and polymer matrix were simulated at nano and micro scale respectively. The interface region between CNT and polymer matrix was modelled using van der Waals forces. These van der Waals forces and the nodes of the inner surface of the matrix were modelled using 3-D non-linear spring elements whose properties were defined by Lennard-Jones (L-J) potential. Simulations were also performed for the neat polymer resin RVE i.e. not reinforced with CNT. Axial impact loading was applied at one end of the cylinder while zero displacement boundary conditions were imposed at the other end. Their simulations demonstrated that the maximum axial deflection was six times greater for the neat resin as compared to CNTRP. Also, the maximum tensile stress at the fixed end was found higher for the neat resin. Therefore, they

concluded that even a small fraction of 5% by volume of CNTs improves the impact resistance of the polymer matrix.

Odegard et al. [7] assumed perfect covalent bonding between CNT and polymer resin in the presence of poly m-phenylenevinylene (PmPV) oligomers. Shokrieh and Rafiee [36] modelled armchair RVE using equivalent-continuum approach and compared their model with Odegard et al. [7]. They considered van der Waals interactions between the two phases and in order to predict the mechanical behaviour of the CNT/polymer composites, they used equivalent long fiber in place of a straight CNT embedded into a polymer matrix with van der Waals interface region. They found highly non-linear behaviour of their constructed model under tensile loading. They also determined the mechanical properties of the equivalent long fibre consisting of CNT and its interface region.

Karimzadeh et al. [37] modelled both cylindrical and square RVEs to evaluate the effective mechanical properties of CNT-based composites. They developed a formulation based on 3-D elasticity theory. For the estimation of Young's modulus in the axial direction of the RVE and validation of the numerical solutions, an extended rule of mixtures was derived. They found that the modulus of elasticity can be increased 10 times with only 5% of nanotube reinforcement. For further research they highlighted that large simulation models for CNT based composites should be developed, which can link nano-, micro- and macroscale models together.

2.4. Modelling Interface between SWNT and Polymer Matrix

Efficiency of SWNT reinforcement into the polymer matrix depends upon the phenomena of load transfer from the host matrix to SWNT which is accomplished through an interface region between the two. Therefore, simulation of interface region plays a critical role in understanding the behaviour of CNTRP under different loading conditions. Since experimental studies at such nano scale is a difficult task, therefore, both the mechanical properties and the thickness value of this interface region have not been reported yet [33]–[36]. Different mechanical properties have been proposed by different researchers and given the values of Young's modulus ranging from ten times to that of the polymer resin to one tenth of the same reflecting hard to soft interfaces [33], [35], [38]. Ayatollahi et al. [33] have used values of 20 GPa, 2 GPa and 0.2 GPa for the Young's modulus of interface region to study the effect of interface stiffness on the RVE behavior. Their results suggest that the Young's modulus of 20 GPa has the minimum influence

on axial stiffness i.e. 10%. Therefore same value has been adopted for modelling interface region of RVE in the current research. Also, there is a huge inconsistency in the data found in literature for outer radii of this region varying from 1 to 9 times the SWNT radius [33], [35], [37], [39], [40]. Ayatollahi et al. [33] arbitrarily assumed the outer radius of interface region as three times the SWNT radius. For the present study, an outer radius of the interface is taken as twice of the SWNT radius.

Chapter 3

EQUIVALENT-CONTINUUM MODELLING OF SINGLE-WALLED CARBON NANOTUBES

Varied experimental and simulation results on the mechanical properties of CNTs have been reported by various researchers and scientists since its emergence. Some of which are discussed above in Section 2.1 to explain the necessity of further research in this highly competitive area. The prime objective of the first half of this research is to investigate the effects of size including diameter and thickness of the nanotube and its chirality on the mechanical properties of SWNTs through equivalent-continuum modelling. Work shown in this chapter directly builds on the work performed earlier by [23], [31], [41] and further elaborated as follows:

i. Tserpes and Papanikos [31] identified the C-C bond thickness and equivalent Young's and shear modulus of the bond for finite element modelling by using the steric potential-mechanical strain energy equivalence. The diameter and thickness value is taken equal as 0.147 nm which is similar to the bond length equal to 0.142 nm. However the expressions for mechanical strain energies used by the authors are linked to slender beams in which case effect of shear deformation and Poisson's ratio of the material are ignored. Therefore, for thick beam, their assumption is invalid. Also, Poisson's ratio of the C-C bond's equivalent material varies between -1 and 0.5 for isotropic and thermodynamically stable materials [42]. Tserpes and Papanikos determined the Young's modulus and shear modulus of the beam element as 5.59 TPa and 0.871 TPa respectively for isotropic material which gives an equivalent Poisson's ratio of 2.15. Their value for Poisson's ratio is above the limit of 0.5 and can be taken in case when the equivalent material of the bond is considered anisotropic [43]. Based on these reservations, Scarpa and Adhikari [41] developed a formulation for the aforementioned mechanical properties of the equivalent C-C bond which behaves like structural element with negligible lateral deformation under stretched conditions. SWNTs simulated in this study are based on these formulations which is applied less or almost none up till now for the evaluation of mechanical properties of the CNTs.

ii. A novel 3D beam element model is proposed in the present work to draw new conclusions regarding Young's modulus, shear modulus, and shear strain for a range of SWNTs.

iii. As mentioned earlier, Xiao et al. [23] and a few others evaluated the mechanical properties of armchair and zigzag nanotubes only and demonstrated the effect of nanotube diameter on the Poisson's ratio of these two types of SWNTs. Current study includes the effect of nanotube diameter and chirality on the Poisson's ratio of not only armchair and zigzag but also chiral structures.

iv. Some of the studies including [4] and [31] perform parametric analysis to investigate the effect of wall thickness on the Young's modulus of CNTs. This research quantifies the relation between the two by providing an equation valid for a range of wall thicknesses found in literature.

The finite element model is built using MSC Marc/Mentat 2010, which is a multi-physics simulation software for nonlinear finite element analysis of static and dynamic problems in particular. The FE models are used to achieve aforementioned aims and objectives. The results obtained are in good agreement with the published data in literature based on other models constructed with other commercial FE software as in [4], [34], [35].

3.1. Equivalent-Continuum Modelling of SWNTS

3.1.1. Linkage between Molecular and Structural Mechanics of SWNTs

Carbon atoms of SWNTs are bonded together by strong covalent bonds and the displacement of each carbon atom is restrained by these bonds under the application of external forces. The total force on each atomic nucleus is determined by the addition of electrostatic force between the positively charged nuclei themselves and the force bred by the electrons [4]. CNTs or SWNTs in particular can be observed as large molecules consist of carbon atoms in molecular mechanics. Total steric potential energy *'Vt'* between the SWNTs' C-C bonds under slight linear elastic deformations, ignoring the electrostatic interactions, can be stated as the sum of following energies [4], [29], [31], [41]:

$$V_t = V_r + V_\theta + V_\tau + V_w \tag{3.1}$$

where *'V_r'*, *'V_θ'*, *'V_τ'* and *'V_w'* are the energy due to bond stretching, energy due to bond angle variation or bending, combined energy due to dihedral angle *'φ'* and out-of-plane torsion *'ω'* and energy due to van der Waals interactions respectively. Figure 3.1 demonstrates the schematic of the aforementioned interatomic interactions in molecular mechanics. First four terms of the Equation 3.1 contributes majorly towards the total steric energy for covalent systems where the effects of energy due to van der Waals interactions are often omitted [4], [41]. The harmonic representation of the each remaining energies is given as [4], [30], [31], [41]:

$$V_r = \frac{k_r (\Delta r)^2}{2} \tag{3.2}$$

$$V_\theta = \frac{k_\theta (\Delta \theta)^2}{2} \tag{3.3}$$

$$V_\tau = \frac{k_\tau (\Delta \varphi)^2}{2} \tag{3.4}$$

where *'k_r'*, *'k_θ'* and *'k_τ'* are the bond stretching force constant, bond angle variation force constant and torsional stiffness force constant respectively. *'Δr'*, *'$\Delta \theta$'* and *'$\Delta \varphi$'* indicate bond stretching variation, in-plane increment, and twisting angle increment respectively. The value for *'k_r'* is taken as 652 nN/nm, for *'k_θ'* as 0.876 (nN nm)/rad^2 and for *'k_τ'* as 0.278 (nN nm)/rad^2, as adopted from Li and Chou [30]. If C-C bonds are considered to act as uniform three dimensional beams capable of stretching, bending and twisting, then the strain energies allied with pure axial and torsion loading can be stated as [4], [30], [31], [41]:

$$V_{stretch} = \frac{EA(\Delta L)^2}{2L} \tag{3.5}$$

$$V_{bend} = \frac{EI(2\alpha)^2}{2L} \tag{3.6}$$

$$V_{twist} = \frac{GJ(\Delta \beta)^2}{2L} \tag{3.7}$$

where *'E'*, *'G'*, *'I'*, *'J'*, *'L'*, and *'A'* represents the equivalent Young's modulus, shear modulus, moment of inertia, polar moment of inertia, length of the beam taken as 0.142 nm equal to length of the C-C bond, and cross-sectional area respectively. Also, *'ΔL'* is the axial deformation due to stretching, *'2α'* is the change in rotational angle, and *'$\Delta \beta$'* is the end beam rotation.

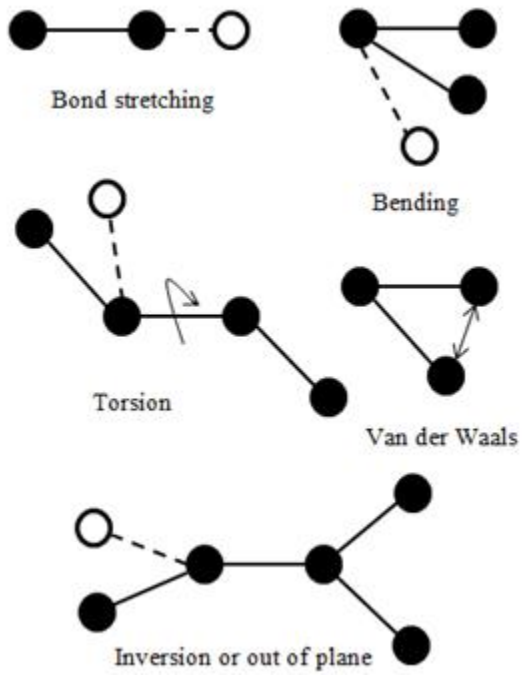

Figure 3.1 Schematic of interatomic interactions in molecular mechanics

Equation 3.6 agrees upon a slender uniform beam under pure bending condition but for thick beams, shear deformation of the cross sectional area under bending condition should be taken into account not to overrate the deflection of the beam. Therefore, to calculate the equivalent continuum diameter of the C-C bond, shear deformation and Poisson's ratio of the equivalent continuum material replacing the covalent bonds should be considered [41]. This consideration by Scarpa and Adhikari [41] deviate the methodology developed by Tserpes and Papanikos [31] into a different direction. Assuming the cross sectional area *'A'* of the beam being circular and isotropic with its diameter *'d'*, the geometric properties can be expressed as [4], [41]:

$$A = \frac{\pi d^2}{4} \tag{3.8}$$

$$I = \frac{\pi d^4}{64} \tag{3.9}$$

$$J = \frac{\pi d^4}{32} \tag{3.10}$$

Scarpa and Adhikari determined the following relations for Young's modulus *'E'* and shear modulus *'G'* from the equivalence between the steric and mechanical strain energies by employing the equivalence between *'Δr'* and *'ΔL'*, also between *'Δβ'* and *'Δθ'* [41].

$$E = \frac{4\, k_r\, L}{\pi d^2} \tag{3.11}$$

$$G = \frac{32\, k_\theta L}{\pi d^4} \tag{3.12}$$

3.1.2. Finite Element Modelling of SWNTs

Scarpa and Adhikari [41] developed an implicit relation between the bond diameter *'d'* and the Poisson's ratio *'ν'* by imposing the isotropic relationship *'G = E/2(1+ν)'* for the equivalent C-C bond medium which enabled them to come up with the sectional properties of the beam element as displayed in Table 3.1.

Table 3.1 Sectional properties of the 3D beam element

Diameter (*d*)	0.0844 nm
Young's Modulus (*E*)	16.71 TPa
Shear Modulus (*G*)	8.08 TPa
Poisson's Ratio (*ν*)	0.0344

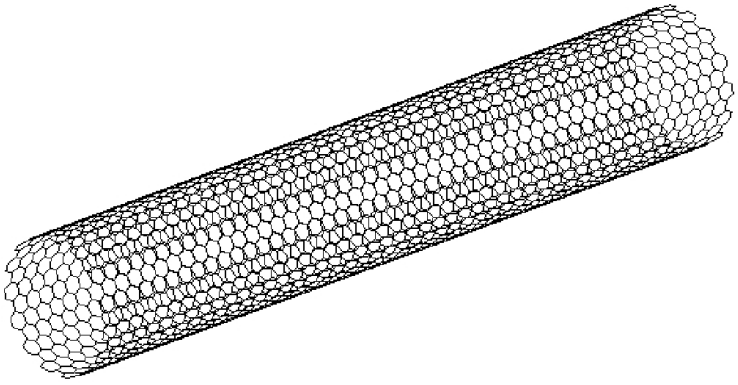

Figure 3.2 Isometric view of the FE mesh of the armchair (15,15) SWNT

Nanoscale FE models of SWNTs are simulated in MSC Marc Mentat 2010 using the sectional properties of the beam element given in Table 3.1. For modelling SWNTs, a 3D solid section beam element (Type 98) is used. The proposed element has six degrees of freedom per each node which are translational, rotational in and about all x, y, and z axes, respectively. It is a straight beam in space including transverse shear effects and is suitable to model linear or non-linear elastic material responses when numerical integration over the cross section is employed. Figure 3.2 displays the isometric view of a FE mesh of the armchair (15,15) SWNT developed with the proposed element. Simulated SWNTs are treated as isotropic materials. Table 3.2 provides the characteristics of all SWNTs brought under investigation in this research (also see Appendix A, Table A.1).

Table 3.2 Characteristics of SWNT models

SWNTS	Diameter (nm)	Chirality (deg)	Length (nm)
Armchair			
(3,3)	0.407	30	12.298
(6,6)	0.814	30	12.052
(10,10)	1.356	30	12.052
(12,12)	1.627	30	12.052
(15,15)	2.034	30	12.052
Zigzag			
(6,0)	0.470	0	12.354
(11,0)	0.861	0	11.928
(15,0)	1.174	0	12.354
(20,0)	1.566	0	12.354
(25,0)	1.957	0	12.354
Chiral			
(4,2)	0.414	19.1	13.525
(8,4)	0.829	19.1	12.398
(12,6)	1.243	19.1	12.398
(16,8)	1.657	19.1	12.398
(20,10)	2.071	19.1	12.398

3.2. Simulation Results and Discussion

3.2.1. Evaluation of Young's Moduli of SWNTs

3.2.1.1. Young's Modulus of Graphene Sheet

A model for graphene sheet is developed using the proposed 3D beam elements and investigated under uniaxial loading as shown in Figure 3.3. The graphene sheet is constrained from one end and given a displacement of 0.1 nm at the other end to perceive the structural responses. Wall thickness *'t'* is taken as 0.34 nm in order to define the cross sectional area *'A = W × t'* of the nanotube. The value for wall thickness corresponds to the interlayer distance between graphene layers in graphite material used by several other authors [4], [29], [30], [44], [45]. Young's modulus *'E_g'* for the graphene sheet can be evaluated by the following equation [4]:

$$E_g = \frac{F\ L_o}{W\ t\ \Delta L} \tag{3.13}$$

where *'F'*, *'W'*, *'L_o'* and *'ΔL'* are the total force applied at displaced extremity, width, initial length and change in length of the graphene sheet respectively.

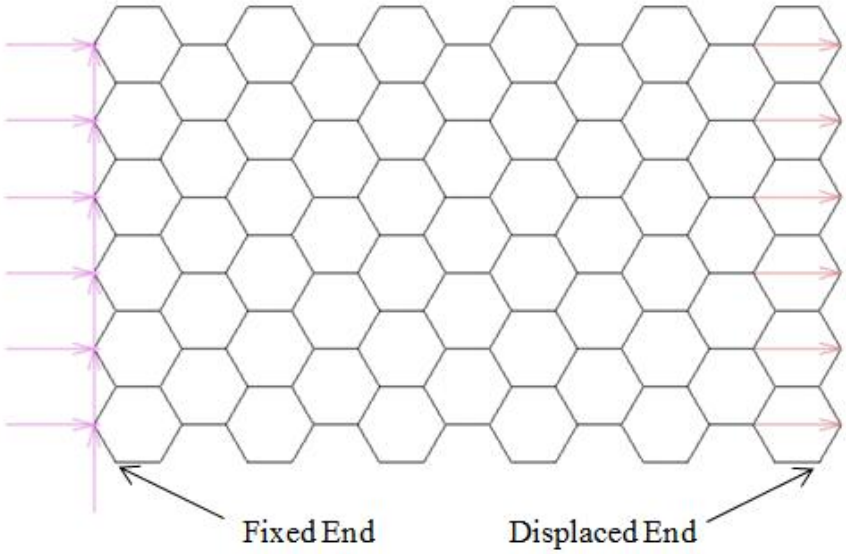

Figure 3.3 FE Model of graphene sheet with boundary conditions

It is observed from the simulation results that length of the graphene sheet does not have any significant effect on its Young's modulus. Therefore, graphene sheets are tested with a fixed length of 10.08 nm and varying widths ranging from 0.74 nm to 23.62 nm. Table 3.3 shows the outcome of the simulation results which are graphically represented as in Figure 3.4. It is observed from Figure 3.4 that as the width to length ratio increases; Young's modulus of the graphene sheet also increases and reaches a plateau at approximately 0.88 TPa. The value is in agreement with those found in literature [4], [26], [29], [46]–[49] validating the proposed 3D beam model to be used for the rest of the analysis. No rotation of the bond and out of plane displacement is observed during the simulations.

Table 3.3 Characteristics of graphene sheet FE models

Width, *W* (nm)	Length, *L* (nm)	*W/L*	*ΔL* (nm)	*F* (nN)	*E* (TPa)
0.74	10.08	0.07	0.10	1.91	0.77
1.48	10.08	0.15	0.10	4.09	0.82
2.95	10.08	0.29	0.10	8.48	0.85
5.90	10.08	0.59	0.10	17.24	0.87
11.81	10.08	1.17	0.10	34.95	0.88
23.62	10.08	2.34	0.10	70.12	0.88

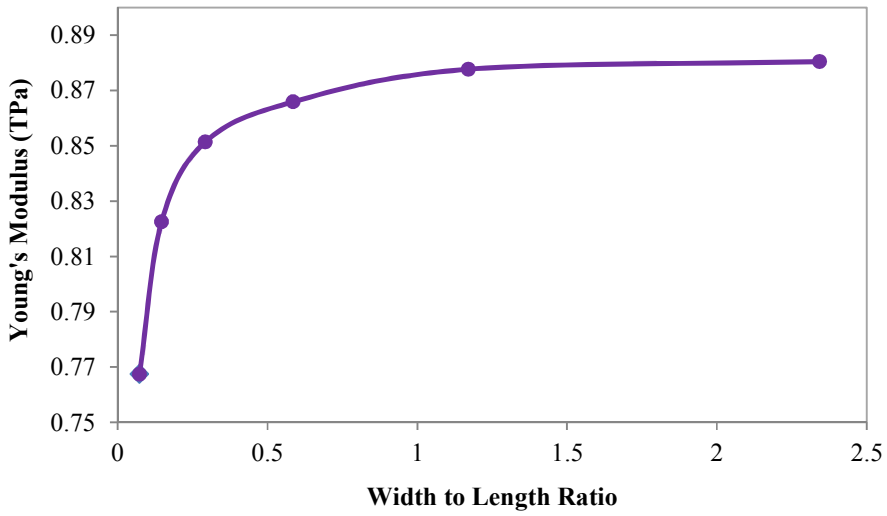

Figure 3.4 Effect of width to length ratio on the Young's modulus of the graphene sheet

3.2.1.2. Effect of Diameter and Chirality on Young's Moduli of SWNTs

The mechanical properties of CNTs depend on their diameter and chirality. The aforementioned FE models are employed to evaluate the effect of diameter and chirality on the Young's moduli of SWNTs. These SWNTs are restrained from one extremity bearing zero displacement and rotation while a displacement of 0.1 nm is applied at the other extremity. Figure 3.5 illustrates the model mesh for armchair (6,6), chiral (8,4), and zigzag (11,0) having similar diameters with the imposed boundary conditions. Figure 3.6 displays the simulation results for zigzag (11,0) showing the displacement in longitudinal direction. Young's moduli *'E'* of SWNTs are determined by the following equation [4]:

$$E = \frac{F\ Lo}{\pi\ d_{cnt}\ t\ \Delta L} \tag{3.14}$$

where *'d_{cnt}'* is the mean diameter of SWNTs. Cross sectional area of SWNT i.e. *'$A_o = \pi\ d_{cnt}\ t$'* is further explained and illustrated in Section 3.2.2.1.

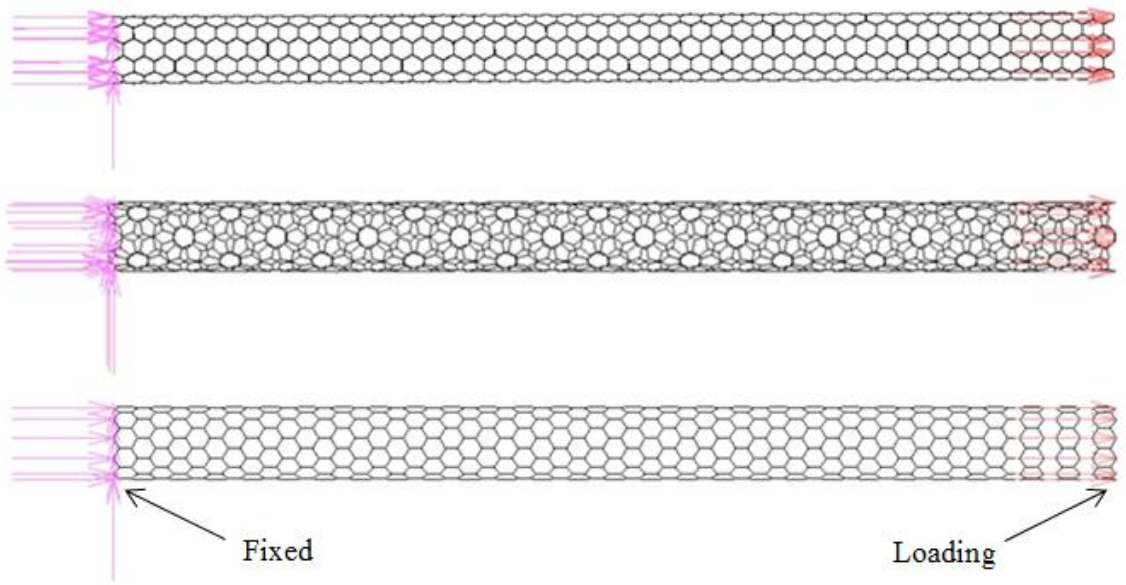

Figure 3.5 Imposed boundary conditions on the armchair (6,6), chiral (8,4) and zigzag (11,0) SWNTs

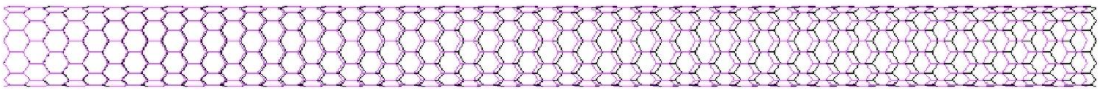

Figure 3.6 Simulation results of the displacement load applied to zigzag (11,0) SWNT in longitudinal direction (deformed and undeformed both shown)

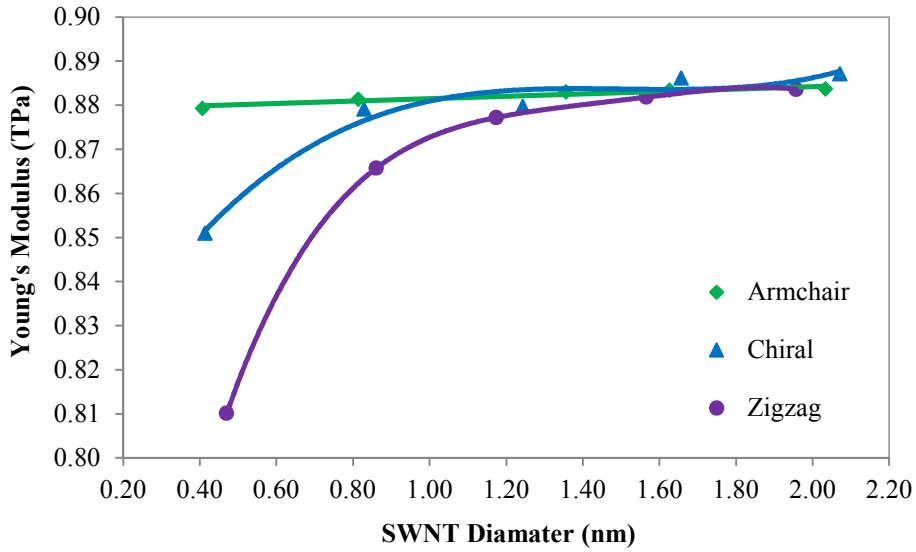

Figure 3.7 Variation of Young's moduli with SWNT diameter for armchair, chiral, and zigzag configurations (data fitted by 5th order polynomial regression)

Only armchair and zigzag nanotubes are brought under investigation in majority of the works reported due to the complexity involved with the computational modelling of chiral nanotubes while in the current work, all the three types of SWNTs are examined and compared against each other. Figure 3.7 shows the variation of Young's moduli of armchair, chiral, and zigzag SWNTs with varying nanotube diameters (also see Appendix B, Table B.1). It is evident from the figure that there is a significant effect of diameter on the Young's moduli of chiral and zigzag SWNTs while no significant effect is observed on the moduli of armchair SWNTs. Young's moduli increase with increasing diameter of chiral and zigzag SWNTs especially for small diameters. This upsurge is due to the influence of nanotube curvature as pointed out by Li and Chou [46]. Curvature increases as the nanotube diameter decreases causing a large distortion of the C-C bonds and therefore, in large displacement of nanotube. As the nanotube

diameter increases, the effect of curvature weakens and the Young's moduli of SWNTs approaches to that of the graphene sheet (0.88 TPa) for which the effect of curvature diminishes completely. Young's moduli of armchair SWNTs are concluded to be the greatest followed by chiral, and then zigzag SWNTs. Young's moduli for all the three types of SWNTs converge to a similar value once the diameter reaches approximately 1.5 nm.

Table 3.4 Comparison on the averaging Young's moduli of all SWNT configurations with diameters below 1.5 nm

Configuration	Chiral Angle (deg)	E (TPa)
Armchair	30	0.881
Chiral	19.1	0.870
Zigzag	0	0.851

Table 3.5 Comparison on the averaging Young's moduli of SWNTs with the reported values

Reference	Diameter (nm)	E (TPa)
Krishnan et al. [50]	1.0-1.5	~1.35
Hernandez et al. [44]	-	~1.24
Jin and Yuan [45]	-	~1.238
Xiao et al. [23]	-	~1.13
Li and Chou [30]	-	~1.06
Yakobson et al. [25]	-	~1.06
Popov et al. [51]	-	~1.0
Lu and Hu [4]	0.375-1.8	0.989-1.058
Ávila and Lacerda [52]	0.391-2.03	0.978-1.057
Meo and Rossi [29]	0.391-2.713	0.897-0.923
This Work	0.407-2.071	0.810-0.887

All SWNTs shown in Table 3.2 are wisely nominated to study the effect of chirality on the Young's moduli. Armchair, chiral, and zigzag SWNTs possess chiral angles of 30^{o}, 19.1^{o} and 0^{o} respectively. Chiral effects of each type of nanotube are studied and compared against the other

two types having approximately similar diameters. As the values for Young's moduli of all SWNT configurations are almost same once the diameter reaches 1.5 nm, hence; the chiral effects are insignificant after that. It can be observed from Table 3.4 that for diameters below 1.5 nm armchair gets relatively higher Young's modulus on average as compared to chiral whereas zigzag attains the lowest. This can be understood as the larger the chiral angle, greater the Young's modulus for nearly same nanotube diameters. Once the SWNT diameter reaches about 1.5 nm, all configurations give a similar Young's modulus. Similar trends are reported by Meo and Rossi [29] and Yakobson et al. [25]. Also, the values of Young's modulus computed in this research are close to those reported in literature as shown in Table 3.5.

Table 3.6 Different values of wall thickness in literature

Reference	Method	Wall Thickness (nm)
Yakobson et al. [25]	MD	0.066
Xin et al. [53]	Tight-binding	0.074
Tu and Ou-Yang [54]	Local density approximation	0.075
Kudin et al. [55]	ab initio	0.089
Tserpes and Papanikos [31]	ECM	0.147
Li and Chou [30]	Structural mechanics	0.34
Jin and Yuan [45]	MD	0.34
Hernandez et al. [44]	Tight binding MD	0.34
Lu and Hu [4]	ECM	0.34
Odegard et al. [28]	ECM	0.69

3.2.1.3. Effect of Wall Thickness on Young's Moduli of SWNTs

The exact values of SWNT thickness at equilibrium state is still under examination. SWNTs are simulated as space-frame structure in the present study and thickness should be specified for the evaluation of Young's modulus. A range of 0.066 to 0.69 nm of wall thickness values are reported in the literature previously as shown in Table 3.6 and the most assumed value is the interlayer spacing of graphite i.e. 0.34 nm. Odegard et al. [28] claimed that thickness is considerably larger than 0.34 nm by combining FE modelling with MD and ECM and proposed values of 0.57 and 0.69 nm for different load cases. However, Pantano et al. [27] used

continuum shell modelling and reported the value of wall thickness to be 0.075 nm. Due to the higher level of uncertainty that exists for the exact values of SWNT wall thickness and wide scatter of the values published in the literature, it is essential to execute a parametric study in order to examine the effect of wall thickness on the Young's modulus of SWNTs.

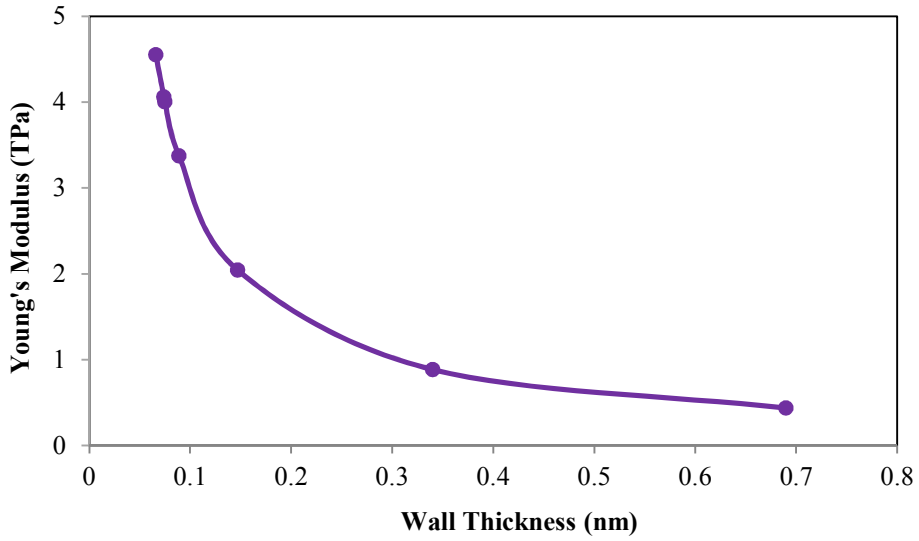

Figure 3.8 Variation of Young's modulus of armchair (10,10) SWNT with wall thickness

Using finite deformation continuum model, Gao and Li [56] established an inverse relation between the Young's modulus of SWNTs and their cross sectional area. Same trends are obtained by Lu and Hu [4], Odegard et al. [28], Tserpes and Papanikos [31], and Ávila and Lacerda [52]. Figure 3.8 presents the similar pattern for armchair (10,10) SWNT confirming that Young's modulus decreases with the increase in wall thickness values. Since there is an inverse relation between the two variables, equation quantifying the relationship valid for a range of wall thicknesses found in literature is proposed as follows:

$$E = \frac{C_{wt}}{t} \tag{3.15}$$

where *'C_{wt}'* is a constant calculated as 0.3002 TPa/nm for the armchair (10,10) SWNT. Value of this constant is specific to each nanotube and on average it is found to be 0.297 TPa/nm for all the SWNT models developed in this study. Equation 3.15 eliminates the dispute of wall thickness and the product of Young's modulus and wall thickness can be taken as the average

elastic modulus *'Et'* of SWNT. Validation is done by comparing with different data coming from distinct approaches. The value of the average elastic modulus is close to those found in literature and summarized a few in Table 3.7. For the sake of comparison with other computational works added to the literature previously, the most commonly used value of 0.34 nm is adopted for the wall thickness *'t'* and used in all the parametric studies conducted in this research.

Table 3.7 Comparison on the averaging Young's moduli *'Et'*

Reference	Method	*Et* (TPa nm)
Hernandez et al. [44]	Tight binding	0.422
Xin et al. [53]	Tight binding	0.377
Yakobson et al. [25]	MD	0.363
Pantano et al. [27]	ab initio	0.363
Tserpes and Papanikos [31]	ECM	0.352
Lu and Hu [4]	ECM	0.349
Li and Chou [30]	Structural mechanics	0.343
Kudin et al. [55]	ab initio	0.343
Odegard et al. [28]	ECM	0.342
Ávila and Lacerda [52]	Molecular mechanics	0.342
Lu [57]	MD	0.331
This Work	ECM	0.297

3.2.2. Evaluation of Shear Moduli of SWNTs

3.2.2.1. Effect of Diameter and Chirality on Shear Moduli of SWNTs

The FE models are used to evaluate the effect of diameter and chirality on the shear moduli of SWNTs. One extremity of the SWNTs are completely restrained bearing zero displacement and rotation while a torsion of 0.1 nN nm is applied to each node in longitudinal direction at the other extremity similar to the fashion applied for the evaluation of Young's moduli shown in Figure 3.5. Figure 3.9 demonstrates the simulation results of zigzag (15,0) SWNT showing the twist in it. Shear moduli *'G'* of SWNTs are evaluated by the following equation [30]:

$$G = \frac{TL}{J\emptyset} \tag{3.16}$$

where *'L'* is the length of SWNT, *'T'* is the total torsional load applied, *'Ø'* is the torsional angle, and *'J'* is the polar moment of inertia of the cross-sectional area. Considering SWNTs as hollow tubes of diameter *'d'* and thickness *'t'* as shown in Figure 3.10, *'J'* is calculated by the following equation [31]:

$$J = \frac{\pi}{32}[(d+t)^4 - (d-t)^4] \tag{3.17}$$

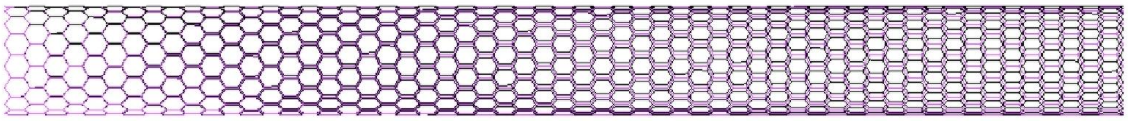

Figure 3.9 Simulation results of torsional load applied to one extremity of armchair (15,0) SWNT in longitudinal direction (deformed and undeformed both shown)

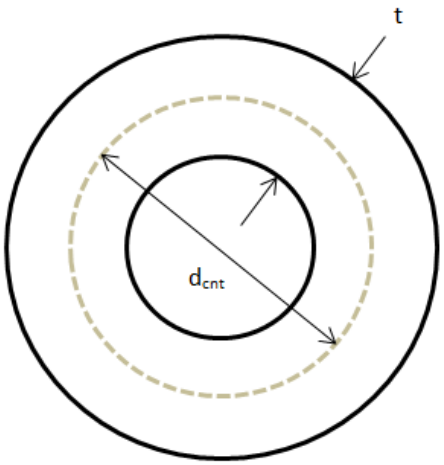

Figure 3.10 Schematic representation of the cross-section of a SWNT

Figure 3.11 shows the variation of shear moduli of armchair, chiral, and zigzag SWNTs with changing nanotube diameters (also see Appendix B, Table B.2). It is obvious from the figure that there is a significant effect of diameter on the shear moduli of all armchair, chiral, and zigzag configurations especially for the small diameters. Shear moduli increase with increasing diameter due to the same effect of curvature which is a function of nanotube diameter. For large diameters of SWNTs, the shear modulus starts forming a plateau and converges to a similar

value. Due to the small size of CNTs, it is difficult to determine its shear modulus experimentally. Therefore, no reliable value for the shear modulus of CNTs has been reported yet through experiments [4], [31]. The values for shear modulus of these CNTs come from computational modelling which is also not much studied when compared to Young's modulus. From the FE models developed in this study, novel trends for the shear modulus of SWNTs are observed. Shear modulus of chiral configuration is concluded to be the largest followed by armchair SWNTs while that of zigzag SWNTs is the lowest. However, for small diameters of SWNTs below 1 nm, shear modulus of zigzag configuration is found to be greater than that of armchair type.

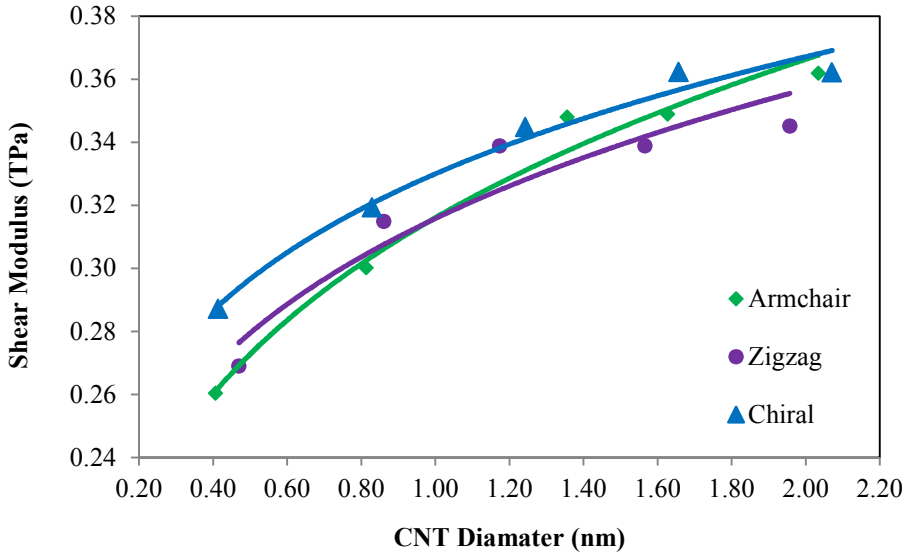

Figure 3.11 Variation of shear moduli with SWNT diameter for armchair, chiral, and zigzag configurations (data fitted by power regression)

Chiral effects of each SWNT configuration are also studied for their shear moduli and compared against the other two configurations having approximately similar diameters. As stated earlier and can be observed from Table 3.8 that on an average chiral gets relatively higher shear modulus as compared to the remaining two. Since carbon atoms in both armchair and zigzag SWNTs are periodically distributed along both angular and axial directions which could cause shear moduli of the two being low in comparison with chiral SWNTs which are not periodically distributed in either angular or axial directions. Similar trends for armchair and zigzag are

observed by Li and Chou [30] and Popov et al. [51] but chiral SWNTs were not studied in their research. The values of shear moduli computed in present work are in good agreement with those reported in literature as shown in Table 3.9.

Table 3.8 Comparison on the averaging shear moduli of all SWNT configurations

Configuration	Chiral Angle (deg)	G (TPa)
Armchair	30	0.324
Chiral	19.1	0.335
Zigzag	0	0.321

Table 3.9 Comparison on the averaging shear moduli of SWNTs with reported values

Reference	Diameter (nm)	G (TPa)
Lu [57]	-	~0.5
Popov et al. [51]	-	0.398
Lu and Hu [4]	0.391-2.07	0.237-0.469
Li and Chou [30]	0.4-2.1	0.25-0.486
This Work	0.407-2.071	0.228-0.360

3.2.2.2. Effect of Diameter and Chirality on Shear Strain in SWNTs

Since the shear moduli calculated in the previous section are aligned with the values available in literature, it gives a new direction to analyze shear strain in SWNTs for which no new simulations are required and can be assessed directly based on the results of shear modulus evaluation. Shear strain *'γ'* in SWNTs is evaluated by the following equation [58]:

$$\gamma = \frac{r\emptyset}{L} \tag{3.18}$$

where *'r'* is the radius of SWNT while the remaining variables have their usual meanings as in Section 3.2.2.1. Figure 3.12 shows the variation of shear strain of all SWNT configurations with varying nanotube diameters (also see Appendix B, Table B.3). A significant effect of diameter on the shear strain in SWNTs is observed especially for the small diameters. Shear strain

decreases with increasing diameter due to the fact that under constant torsional load application, angular variation in the large diameter nanotubes decreases. Also, as the elastic moduli of SWNTs increase, it can be anticipated that shear strain will decrease due to less axial and angular deformation under constant loading. It is evident from Table 3.10 that shear strain in SWNT configurations is approximately same; hence, chiral effects are found insignificant in this case.

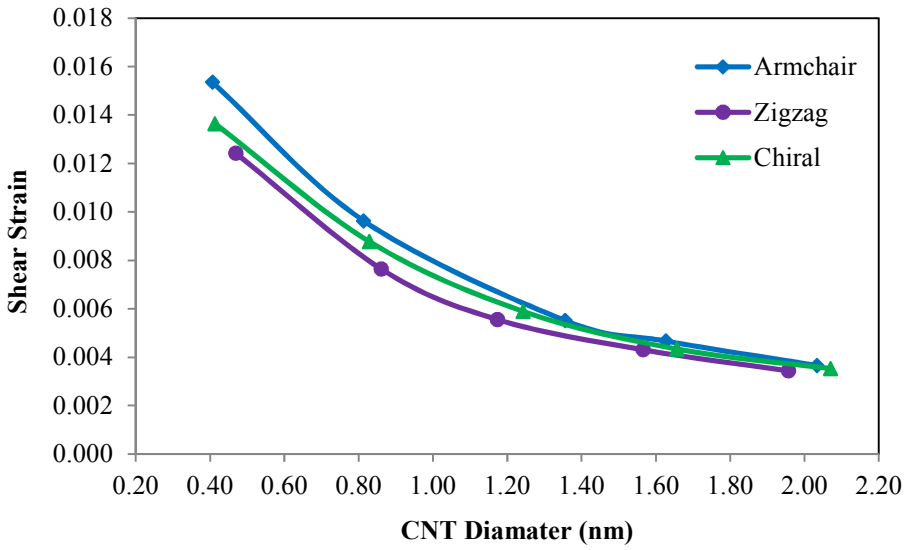

Figure 3.12 Variation of shear strain with SWNT diameter for armchair, chiral, and zigzag configurations

Table 3.10 Comparison on the averaging shear strain in all SWNT configurations

Configuration	Chiral Angle (deg)	γ
Armchair	30	0.008
Chiral	19.1	0.007
Zigzag	0	0.007

3.2.3. Evaluation of Poisson's Ratio of SWNTs – Effect of Diameter and Chirality

In order to study the effect of diameter and chirality on the Poisson's ratio of SWNTs, FE models are given an axial displacement of 1 nm to each node in longitudinal direction at both

the extremities. Figure 3.13 demonstrates the simulation results of armchair (10,10) showing the change in diameter of SWNT due to the axial displacement. Poisson's ratio *'ν'* of SWNTs are evaluated by the following equation [37]:

$$\nu = -\frac{\Delta d}{d} \times \frac{L}{\Delta L} \tag{3.19}$$

where *'Δd'* and *'ΔL'* are the change in diameter and length respectively due to the application of axial load at the outer most nodes of SWNTs.

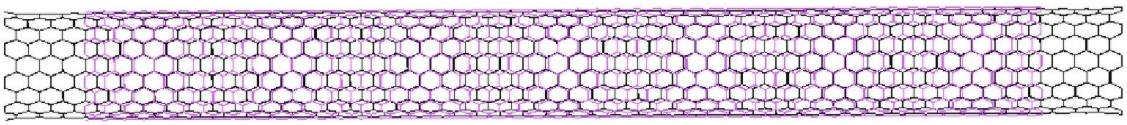

Figure 3.13 Simulation results of tensile load applied to both extremities of armchair (10,10) SWNT in longitudinal direction (deformed and undeformed both shown)

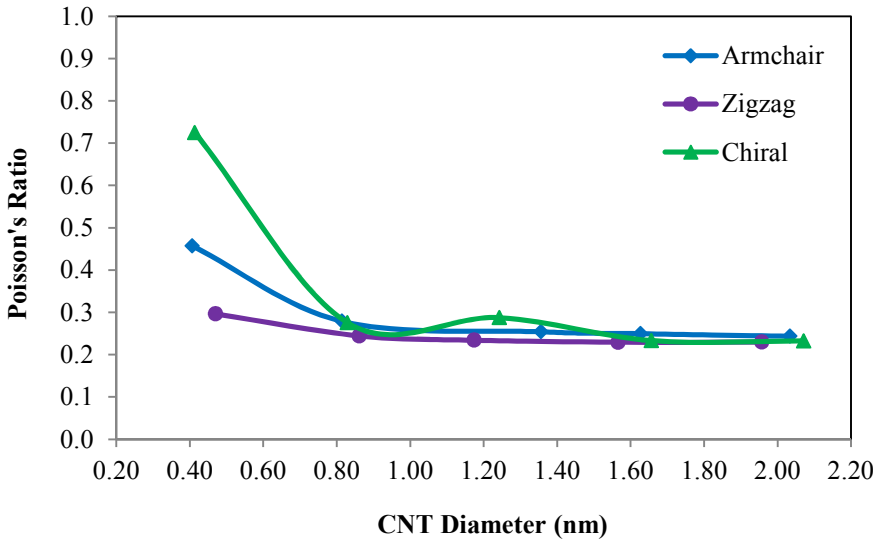

Figure 3.14 Variation of Poisson's ratio with SWNT diameter for armchair, chiral, and zigzag configurations

Figure 3.14 shows the dependence of Poisson's ratio on the SWNT diameter (also see Appendix B, Table B.4). It is clear from the figure that Poisson's ratio for all the SWNT configurations

decreases with increasing diameter, converging to approximately a similar value once the diameter reaches 0.8 nm. This can be concluded as for very low diameter SWNTs, variation in Poisson's ratio exist but for a range of SWNTs that are commercially viable, Poisson's ratio is more or less same. SWNTs are considered highly isotropic, homogenous and cohesive materials but due to their space frame structure, small diameter SWNTs possess large empty spaces with fewer bonds between C-C atoms which adds exception to the variation in values for Poisson's ratio.

Similar to the case of shear strain, chiral effects are also not significant on the Poisson's ratio of SWNTs but for the sake of comparison, the exact values of each nanotube configuration at which it converges are presented in Table 3.11. It can be observed that armchair possesses relatively higher Poisson's ratio followed by chiral whereas zigzag has the lowest. This can be settled as the larger the chiral angle, greater the Poisson's ratio for nearly same nanotube diameters. Similar decreasing and then converging trends for only armchair and zigzag SWNTs are reported by Xiao et al. [23] and Goze et al. [59]. The values of Poisson's ratio calculated in this research are in good agreement with those exist in literature as shown in Table 3.12.

Table 3.11 Comparison on the Poisson's ratio of all SWNT configurations

Configuration	Chiral Angle (deg)	ν
Armchair	30	0.244
Chiral	19.1	0.233
Zigzag	0	0.230

Table 3.12 Comparison on the averaging Poisson's ratio of SWNTs with reported values

Reference	Diameter (nm)	ν
Lu [57]	-	~0.28
Goze et al. [59]	-	~0.262
Popov et al. [51]	-	0.21
Xiao et al. [23]	~0.3-2.8	~0.2
This Work	0.407-2.071	~0.235

Chapter 4

CONTINUUM MODELLING OF CARBON NANOTUBE REINFORCED POLYMER COMPOSITES

This chapter includes modelling of carbon nanotube reinforced polymer composites (CNTRPs) based on continuum approach. The prime objective of the work done in this chapter is to determine the effect of SWNT chirality and diameter on the mechanical properties of the SWNT/epoxy composite which is nearly absent in the literature. For this purpose, this study directly builds on the work performed in the previous chapter. The equivalent beam element introduced earlier to model SWNTs is employed to build SWNT/epoxy composite signified by a cylindrical representative volume element (RVE). Also, different approaches to model these cylindrical RVEs are compared against each other and validated from the values published in literature.

4.1. Modelling Representative Volume Element (RVE)

Three classifications of RVEs i.e. circular, square and hexagonal are found in the literature to model CNT based composites [37]. These classifications are based on the shape of their cross-section as shown in Figure 4.1. These RVEs are essential to provide detailed analyses of SWNTs interacting with the polymer matrix such as mechanisms for load transfer, stress distributions, adhesion of the two phases. In this study, RVEs are modelled using cylinders which are mostly applied by the researchers worked on CNTRP modelling. The RVE developed for this particular study consists of SWNTs reinforced in the polymer (epoxy) resin with an interface region in between the two. The finite element model of the RVE is developed using MSC Marc/Mentat 2010. Constructing RVE is achieved in three different stages of modelling and is outlined as below:

i. Single-walled carbon nanotube
ii. Polymer matrix
iii. Interface region between SWNT and polymer

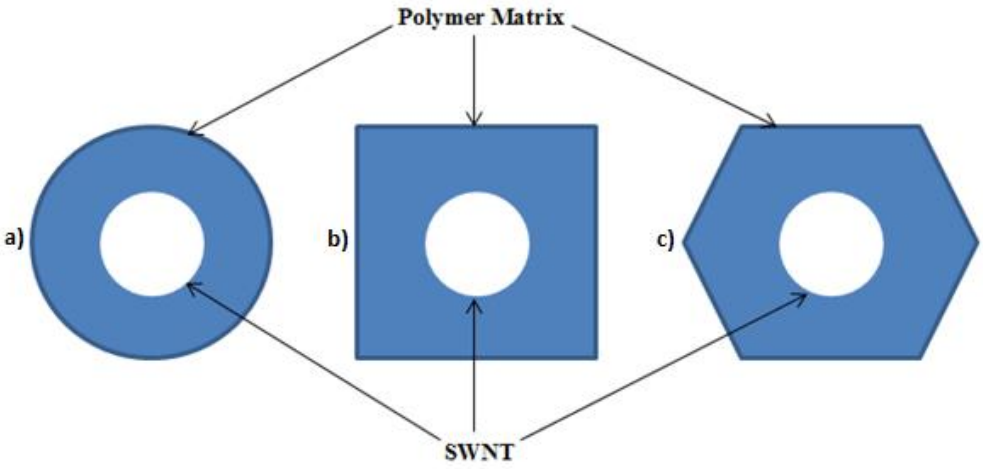

Figure 4.1 Different types of RVE modelling a) circular, b) square and c) hexagonal

First stage of SWNT modelling has already been presented in detail in the previous chapter. A good agreement between the results obtained and the published values encourages proceeding further towards other two modelling stages.

4.1.1. Polymer Matrix

Volume fraction of SWNTs in most of its polymer composites 'V_f' is about 3-5% [36]. Therefore the volume of polymer matrix is much larger as compared to SWNTs in molecular scale. Due to this reason, simulating polymeric chains requires a massive number of elements and computations at nano-scale. However, the molecular chains of the polymers are relatively tighter than SWNTs providing a high density space. As a rational compromise, the surrounding polymer can be simulated as a continuum medium and solid elements can be used for simulations [34]–[36]. Element (7) of the software is used to model polymer matrix.

Element (7) is an eight-node, isoperimetric, arbitrary hexahedral titled as 3D arbitrarily distorted brick. The stiffness of the element is shaped using eight-point Gaussian integration. Further explanation of the element is found in the element library of the Marc Mentat. The size of the element is nominated as lower as the length of hexagonal rings of SWNTs in axial direction. Depth of the polymeric region is calculated in a way that it should reflect a volume fraction of 5% for an embedded SWNT. The simulated polymer matrix is treated as an isotropic material with Young's modulus and Poisson's ratio of 10 GPa and 0.3 respectively. These are the corresponding values for specific Epoxy resins available in the market [36].

4.1.2. Interface Region between SWNT and Polymer Resin

As stated earlier that simulating interface region is critical because the load is transferred from the host polymer matrix to the SWNT via an interface between the two. Other than the issues discussed in Section 2.4, researches have also proposed different types of bonding between SWNT and polymer matrix in their models and the two most assumed approaches are further elaborated in the following two sub-sections. RVEs from both these approaches have been developed in this study for the sake of comparison.

4.1.2.1. Approach 1: Non-bonded Interactions

First approach suggests that the interactions between nanotube and surrounding polymer are weakly non-bonded van der Waals interactions. Functionalisation is a process of introducing covalent crosslinks between the carbon atoms of the SWNTs and the molecules of the polymer to enhance the load transferring capability from the host matrix to SWNTs [60]–[62]. But this process has negative aspects as well causing defects in the structure of SWNTs while forming crosslinks [63], [64]. Therefore, interface region is treated as non-bonded interactions and modelled using van der Waals links.

In this approach, SWNTs and their respective interfaces are modelled as discrete structures while resin is modelled using solid elements. The interface region is developed using truss/spring elements connecting the carbon atoms of discrete SWNTs to the nodes of solid elements representing polymer matrix. Very few of the researchers have applied beam elements for the interface construction. Recently, Wernik and Meguid [65] used multi-linear beam element to develop interface region [35]. In this study, 3D beam elements are employed to model interface as well. Lennard-Jones potential is a mathematical model used to estimate the interactions between neutral atoms or molecules. The properties of these elements are determined using Lennard-Jones (L-J) "6-12" potential resulting into van der Waals forces given by the following equation [66]:

$$F_{vdw} = 4\,\frac{\varepsilon}{r}\left[-12\left(\frac{\sigma}{r}\right)^{12} + 6\left(\frac{\sigma}{r}\right)^{6}\right] \tag{4.1}$$

where *'ε'* and *'σ'* are the Lennard-Jones parameters specific to interactions between C-C atoms and are taken as 0.4492 kJ/mol and 0.3825 nm respectively. *'r'* is the interatomic distance

between the C-C atoms [66]. Equation 4.1 suggests that for interatomic distances greater than 0.85 nm, van der Waals forces approaches to zero. Therefore, interface region has been modelled in a way that beam elements are employed between SWNT atoms and inner surface of the polymer only when the distance between the two is less than or equal to 0.85 nm. The radius of the beam element is taken as 1.7 nm which is the bond radius of the C-C van der Waals link [67]. All the three parts of the resulting CNTRP model with SWNT being armchair (10,10) is shown in Figure 4.2. Interface beam elements representing van der Waals links connecting the nodes of SWNT and the polymer are shown in Figure 4.3.

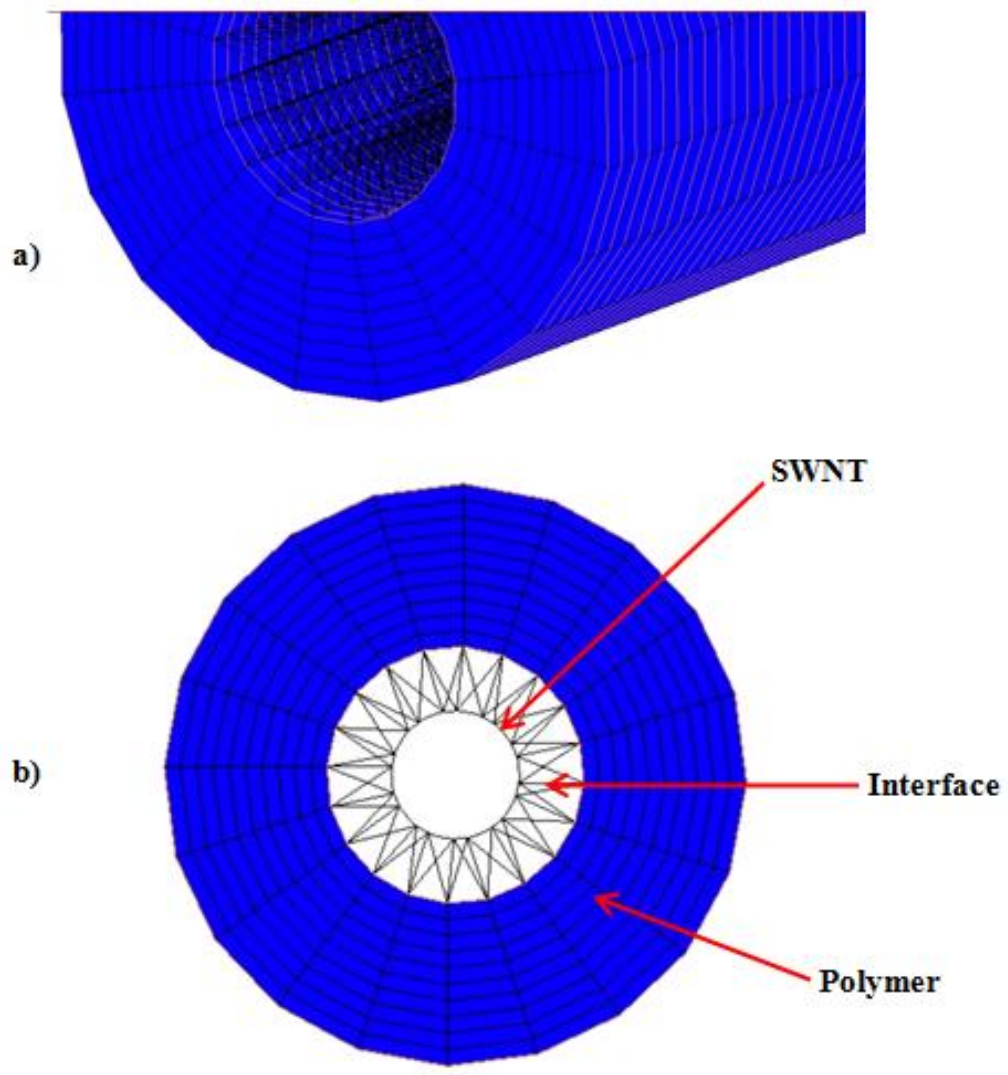

Figure 4.2 a) Isometric view of the RVE model, b) End view of SWNT, weakly bonded interface region and surrounding polymer resin

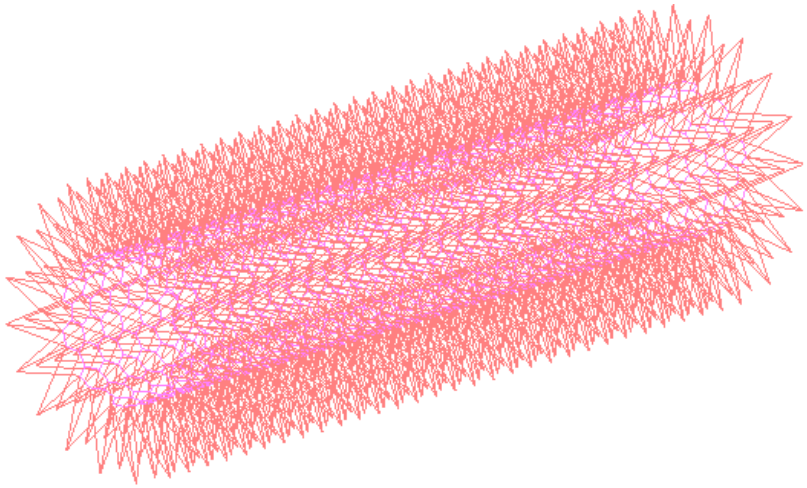

Figure 4.3 Van der Waals links at the interface connecting nodes of SWNT to that of polymer

4.1.2.2. Approach 2: Perfect Bonding Model

Second approach assumes perfect bonding between the SWNTs and the polymer matrix to model these nano-composites using the continuum models. Research has been demonstrated that the possibility of having such a strong C-C bond between the SWNT and polymer exists [37] which creates an opportunity to employ this approach for the modelling purposes. Karimzadeh et al. [37] applied the same approach to model both cylindrical and cuboidal RVEs with an assumption that both the SWNTs and polymer matrix in a RVE are continua of linearly elastic, isotropic, and homogenous materials with given values of Young's moduli and Poisson's ratios. In this study, same assumption has been taken into account. Figure 4.4 shows the cylindrical RVE constructed with solid elements. For the sake of comparison with the previous model, armchair configuration (10,10) is chosen as the reinforcement.

4.2. Models' Verification

Before proceeding with any of the two aforementioned RVE models for the determination of chiral effects, it is important to compare the results of the two models with those found in literature to verify the accuracy of the finite element models. RVEs developed by Approaches 1 and 2 are termed as RVE-1 and RVE-2 respectively.

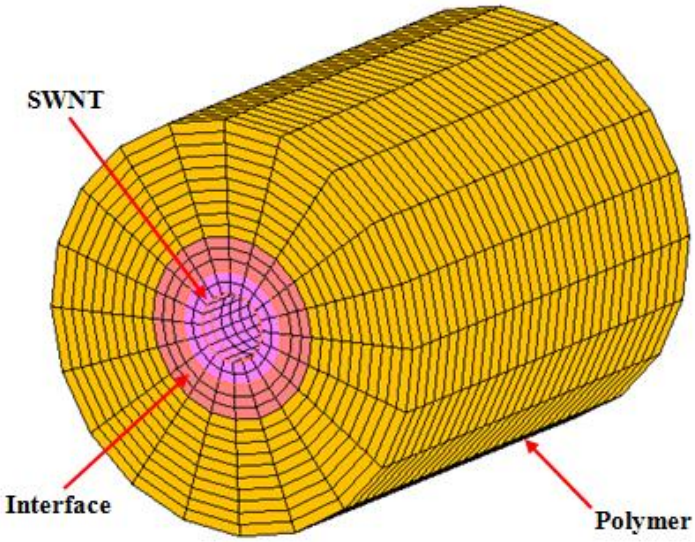

Figure 4.4 FE mesh of cylindrical RVE with all solid elements

4.2.1. Tensile Stress-Strain Behavior of RVE-1

For the verification of RVE-1, the tensile stress-strain behavior of the RVE is investigated and compared with the results of Rafiee et al. [34] who modelled their RVE in a fashion similar to this study. Same armchair (10,10) SWNT is embedded into their RVE model as well which provides firm basis to compare the present model with. The boundary conditions used for RVE under axial loading are similar to those used for SWNT alone as shown in Figure 3.5. RVE-1 is restrained from one extremity bearing no displacement and rotations while displacements ranging from 0.1 nm to 1 nm are given to the other extremity to develop the tensile stress-strain curve. Figure 4.5 displays the simulation result of RVE-1 showing the displacement of 0.1 nm in longitudinal direction. The results of the stress-strain behavior of RVE-1 are demonstrated in Figure 4.6. Particularly for small strains both models' stress prediction appears quite close to each other. This reflects the acceptable accuracy of RVE-1. The slope of tensile stress-strain curve shown in Figure 4.6 gives the Young's modulus of RVE-1 as 52.04 GPa.

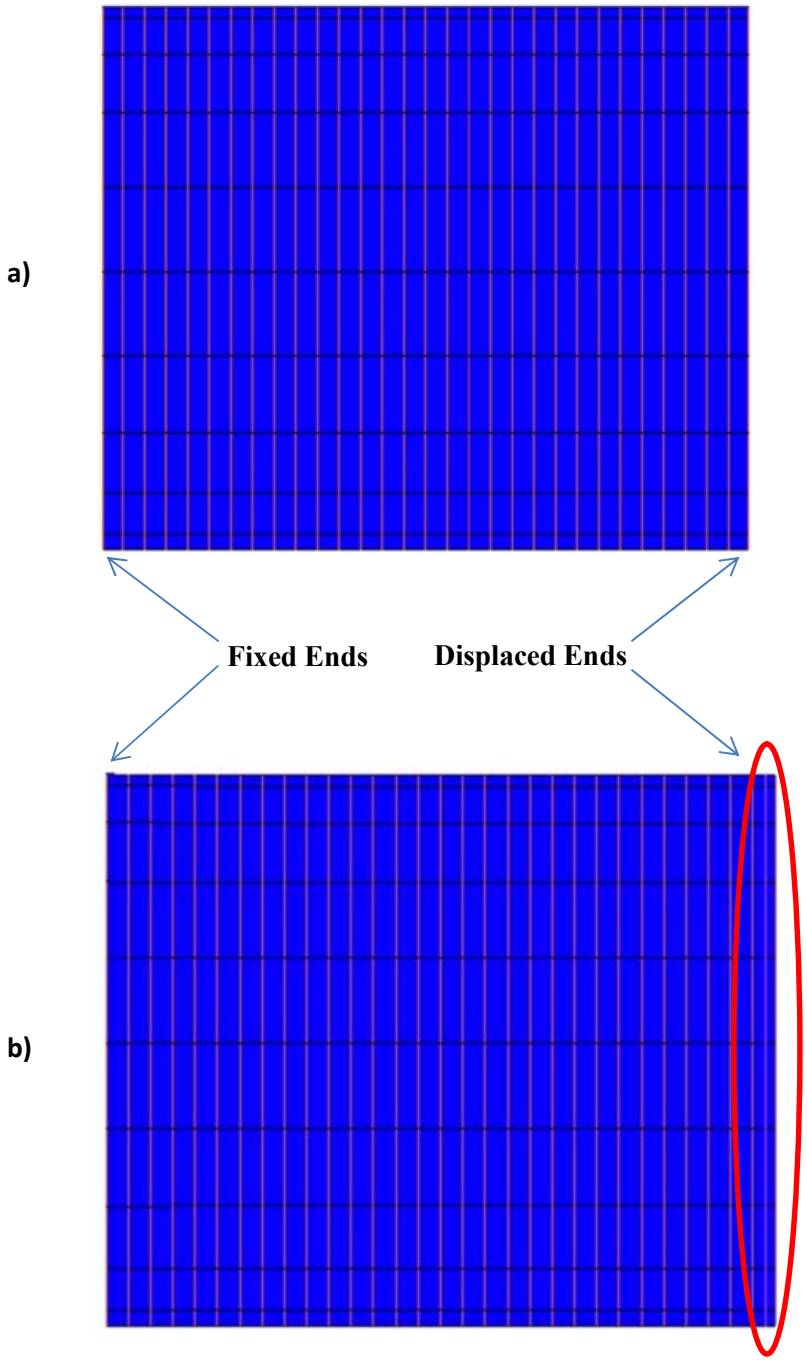

Figure 4.5 Side views of RVE-1 a) before displacement b) after displacement

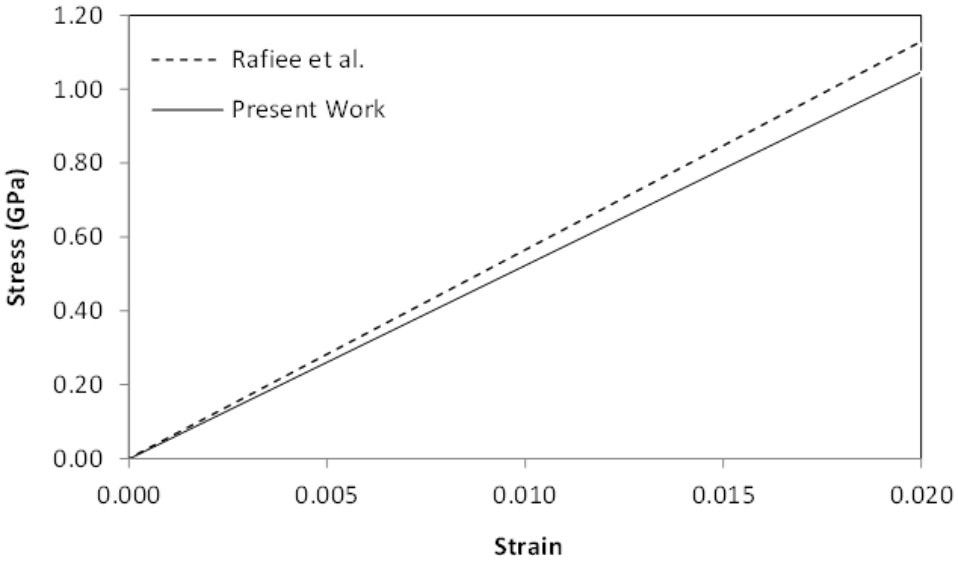

Figure 4.6 Tensile stress-strain behavior of RVE-1

4.2.2. Young's Modulus of RVE-2

For the Young's modulus of RVE-2, one end of the model is completely restrained again while a displacement of 0.1 nm is applied to the other end. Visually the side view of the simulation result of RVE-2 showing the displacement of 0.1 nm in longitudinal direction is same as of Figure 4.5. The effective Young's modulus of RVEs *'E_{RVE}'* under tensile loading is calculated by the following equation [33]:

$$E_{RVE} = \frac{F_{RVE} L_{RVE}}{A_{RVE}\, \Delta L_{RVE}} \tag{4.2}$$

where *'F_{RVE}'* is the reaction force in axial direction, *'L_{RVE}'* is the initial length of RVE, *'ΔL_{RVE}'* is the axial displacement and *'A_{RVE}'* is the cross sectional area of RVE given by *'$A_{RVE} = \pi(R_{RVE}^2 - R^2)$.'* *'$R_{RVE}$'* is the radius of RVE while *'R'* is the inside radius of the SWNT. Cross sectional area of RVE-2 is demonstrated in Figure 4.7. The Young's modulus obtained from the FE simulation of RVE-2 gives a value of 54.470 GPa which is similar to that observed in case of RVE-1. Table 4.1 presents the comparitive study of Young's modulus from both the models developed in this study and those found in literature along with a theoretical relation known as continuum rule of mixtures discussed in Section 4.2.3. A good agreement can be seen with the published data.

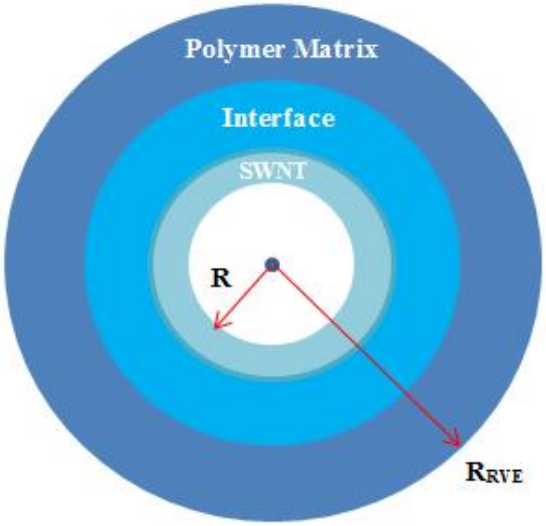

Figure 4.7 Cross-sectional area of RVE-2

Table 4.1 Comparative study on Young's moduli of RVEs with armchair (10,10) reinforcement

Reference	Approach	V_f (%)	E_{RVE} (GPa)
Karimzadeh et al. [37]	Perfect bonding	3	53.46
Rafiee et al. [34]	Perfect bonding	5	56.47
Shokrieh & Rafiee [36]	Non-bonded interaction	5	58.59
Wernik & Meguid [65]	Non-bonded interaction	5	50.30
RVE-1	Non-bonded interaction	5	52.04
RVE-2	Perfect bonding	5	54.47
Rule of Mixtures	-	5	53.65

4.2.3. Validation by Continuum Rule of Mixtures

A large number of theoretical works have been carried out since 1950s for modelling mechanical properties of reinforced composites. In order to show the validity of the results found in this study theoretically, one of the most common technique known as 'continuum rule of mixtures' is used. In the simplest case, composite can be modelled as an elastic, isotropic matrix filled with alligned fiber that span the full length of the composite [68]. In the present study, the matrix and the fibrous material is polymer and SWNT respectively with the same

assumptions as of the simplest case. Hence, it is anticipated to have similar results from both the rule of mixtures and the RVE model simulations. According to the rule, when the stress is applied in the direction aligned to that of SWNT and matrix both will be equally strained and under this circumstance, Young's modulus of the composite is given by the following equation [37], [65], [68]:

$$Ec = E\,Vf + Em(1 - Vf) \tag{4.3}$$

where *'E_c'*, *'E'* and *'E_m'* are the Young's moduli of composite, SWNT and polymer matrix respectively while *'V_f'* is the volume fraction. The strength of the material solution for Young's modulus calculated by Equation 4.3 is found to be 53.65 GPa and listed in Table 4.1 for comparison with the results of RVE simulations. Young's modulus of the composite is similar to the simulation results and lies in between the values determined via two approaches. This creates an opportunity to use any of the two models for the assessment of chiral effects on the mechanical properties of CNTRPs.

Cox [69] introduced a length efficiency factor *'η_l'* into the Equation 4.3 due to the fact that fibers are relatively short in the bulk of the matrix due to which these shorter lengths carry load less efficiently as compared to the long fibres. Also, in many situations these fibers may not be aligned and depends upon the dispersion technique employed for the fabrication of composites. Hence, another parameter called orientation efficiency factor *'η_o'* is often used with Equation 4.3 [68]. As the literature review in Section 2.1 suggests, there is a large diversity in results for CNTRPs experimentally due to different and less efficient dispersion techniques which effects the SWNT orientations and load transfer mechanisms of CNTRPs. Since the values of these efficiencies are not reported in the experimental studies, the results of this study are compared with computational and analytical studies only where the aforementioned efficiencies are considered 100% [37], [65]. Values for Young's modulus determined computationally with efficiencies being maximum, experimental investigators can compare their results with these in order to determine the quality of dispersion they have achieved. The closer their value to the one determined computationally, the better their dispersion is.

4.3. Simulation Results and Discussion

4.3.1. FE Models

Both the models give relatively similar results as shown in the previous section. Hence, due to the complexity involved with the continuum modelling of SWNTs especially chiral configurations using Approach 1, Approach 2 has been employed to study the effects of chirality and diameter of SWNTs on the mechanical properties of CNTRPs represented by their respective RVEs. Sensitivity analysis for the RVE FE meshes employing Approach 2 is presented in Appendix C. As the solid elements accept material properties in the form of Young's modulus and Poisson's ratio only, these two properties are selected to analyze how chirality of SWNT and its size affects the values of the whole composite. Table 4.2 provides the characteristics of all representative volume element models brought under investigation in Section 4.3.2 and 4.3.3. (also see Appendix A, Table A.2).

Table 4.2 Characteristics of RVE Models

Reinforced SWNT	SWNT Diameter (nm)	Chirality (deg)	RVE Diameter (nm)	Length (nm)
Armchair				
(3,3)	0.407	30^o	3.328	7.377
(6,6)	0.814	30^o	4.729	7.377
(10,10)	1.356	30^o	6.158	7.377
(12,12)	1.627	30^o	6.776	7.377
Zigzag				
(6,0)	0.47	0^o	3.578	7.377
(11,0)	0.861	0^o	4.867	7.377
(15,0)	1.174	0^o	5.712	7.377
(20,0)	1.566	0^o	6.641	7.377
Chiral				
(4,2)	0.414	19.1^o	3.357	7.377
(8,4)	0.829	19.1^o	4.774	7.377
(12,6)	1.243	19.1^o	5.884	7.377
(16,8)	1.657	19.1^o	6.841	7.377

4.3.2. Effects of SWNT Diameter and Chirality on Young's Moduli of RVEs

The mechanical properties of CNTRPs depend upon the diameter and chirality of reinforced CNTs into the polymer matrix. All the RVE models shown in Table 4.2 are constrained from one extremity giving zero displacement and rotation and a displacement of 0.1 nm is applied to the other extremity of the models. All the RVEs are of same initial length i.e. 7.377 nm ranging from approximately 4.5 to 18 times of the SWNT diameters investigated in this study. Imposed boundary conditions are same as illustrated in Figure 4.5. Young's moduli of all RVE models are determined by Equation 4.2.

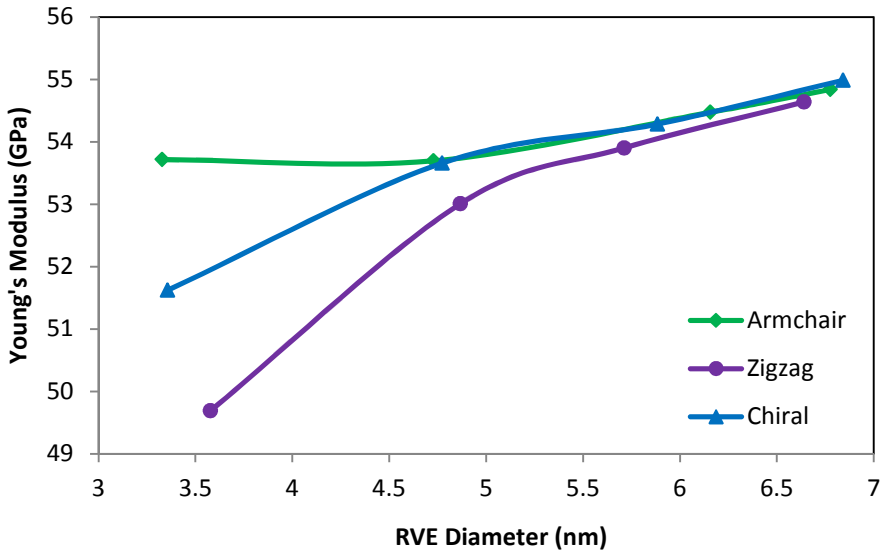

Figure 4.8 Variation of Young's moduli with RVE diameter

As mentioned earlier, effect of SWNT chirality and diameter over the mechanical properties of CNTRPs are not reported earlier. Figure 4.8 demonstrates the variation of Young's moduli of all armchair, zigzag and chiral structures reinforced polymer (epoxy) composites with varying RVE radii (also see Appendix B, Table B.5). It is evident from the figure that there is a significant effect of RVE diameter on the Young's moduli of RVEs having armchair, zigzag and chiral SWNTs embedded into it especially for small diameters. Increase in RVE diameter corresponds to the increase in SWNT diameter. Therefore, Young's moduli of RVEs can be directly correlated with the diameters of SWNTs. As expected, Young's moduli increases with increasing diameter of SWNTs due to the decrease in nanotube curvature, same as in case of

SWNTs only, explained earlier is Section 3.2.1.2. Interestingly, Young's moduli of armchair RVEs also increase although for only armchair SWNTs, Young's modulus remains almost constant. This is due to the fact that increase in armchair diameter increases perfect bonding surface area between armchair and polymer matrix which eventually increases its modulus.

Table 4.3 Evaluation of Young's moduli of RVEs and comparison with rule of mixtures

Reinforced SWNT	RVE Diameter (nm)	Length (nm)	ΔL (nm)	Force (nN)	E_{RVE} (GPa)	E_c (GPa)
Armchair						
(3,3)	3.328	7.377	0.1	6.33	53.71	53.46
(6,6)	4.729	7.377	0.1	12.66	53.69	53.57
(10,10)	6.158	7.377	0.1	21.39	54.47	53.65
(12,12)	6.776	7.377	0.1	25.84	54.83	53.67
Zigzag						
(6,0)	3.578	7.377	0.1	6.76	49.69	50.01
(11,0)	4.867	7.377	0.1	13.22	53.01	52.79
(15,0)	5.712	7.377	0.1	18.32	53.90	53.36
(20,0)	6.641	7.377	0.1	24.78	54.64	53.59
Chiral						
(4,2)	3.357	7.377	0.1	6.19	51.62	52.05
(8,4)	4.774	7.377	0.1	12.88	53.66	53.45
(12,6)	5.884	7.377	0.1	19.54	54.28	53.48
(16,8)	6.841	7.377	0.1	26.38	54.98	53.81

All RVEs shown in Table 4.2 are chosen carefully to have similar diameters for each chiral angle. Embedded SWNTs possess chiral angles of 30^o, 19.1^o and 0^o for armchair, chiral and zigzag configurations respectively. It can be observed from Table 4.3 that on average, Young's moduli of armchair RVEs are concluded to be the most followed by chiral and then zigzag following the same trend as in case of armchair SWNTs only. This concludes that the larger the chiral angle, greater the Young's modulus for almost same RVE diameters. The trends are verified by the continuum rule of mixtures which are also demonstrated in Table 4.3. The values

determined by the rule follow the same trend as of the results determined via simulations validating the observed patterns.

4.3.3. Effects of SWNT Diameter and Chirality on Poisson's Ratio of RVEs

To study the effect of diameter and chirality of SWNTs on the Poisson's ratio of RVEs, FE models are given an axial displacement of 2 nm to each node in longitudinal direction at one extremity while the other extremity is restrained completely bearing no displacement and rotation. Figure 4.9 illustrates the simulation result of RVE having zigzag (15,0) SWNT reinforced into it showing the change in diameter and length of RVE due to the axial deformation. Poisson's ratio *'ν_{RVE}'* of RVEs are evaluated by the following equation [37]:

$$\nu_{RVE} = -\frac{\Delta d_{RVE}}{d_{RVE}} \times \frac{L_{RVE}}{\Delta L_{RVE}} \tag{4.4}$$

where *'Δd_{RVE}'*, *'ΔL_{RVE}'*, *'d_{RVE}'* and *'L_{RVE}'* are the change in diameter and length, initial diameter and length of RVEs respectively.

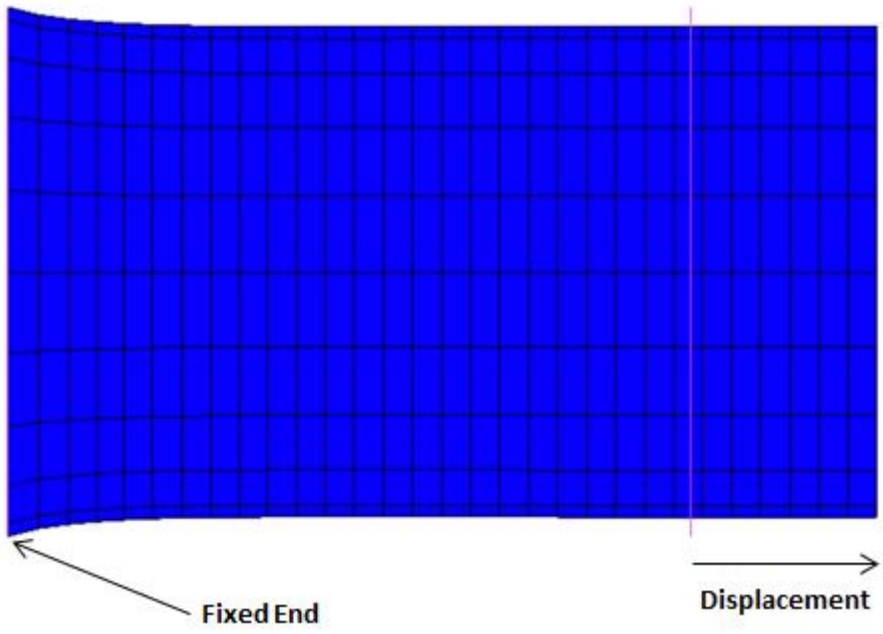

Figure 4.9 Simulation results of tensile load applied to zigzag (15,0) SWNT RVE in longitudinal direction

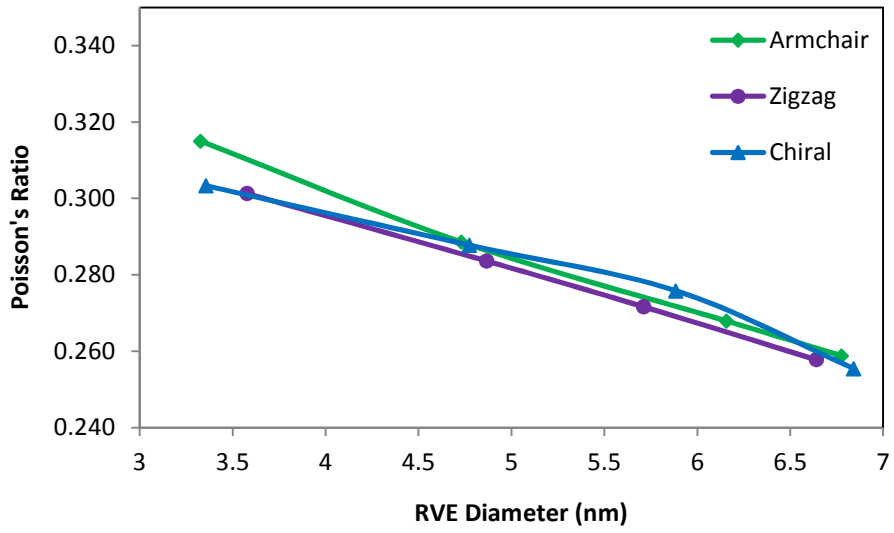

Figure 4.10 Variation of Poisson's ratio with RVE diameter

Effect of diameter is observed not to be much significant in case of SWNTs only but once these are reinforced into the polymer matrix, Poisson's ratio affects significantly. Figure 4.10 demonstrates the dependence of Poisson's ratio on the RVE diameter (also see Appendix B, Table B.6). It is observed from the figure that Poisson's ratio of all the RVEs decreases with increasing diameter. This is due to the nature of polymers undergoing large deformations as compared to the SWNTs resulting into larger strains causing Poisson's ratio to vary substantially. Table 4.4 presents the average values of Poisson's ratio of each RVE type. It can be observed from the table that chiral effects are found to be not much significant. The average value of Poisson's ratio of all RVEs determined in this research are in good agreement with the value of 0.3 reported by Karimzadeh et al. [37].

Table 4.4 Comparison on averaging the Poisson's ratio of each RVE type

Configuration	Chiral Angle (deg)	ν
Armchair	30	0.283
Chiral	19.1	0.281
Zigzag	0	0.279

4.4. Potential Reduction in Structural Mass

Since, this study is aimed towards sustainable development; therefore, a performance parameter called specific stiffness which is mostly used for comparing materials is selected to estimate the impact of replacing neat epoxy resin with epoxy/SWNT composite in its potential applications. Specific stiffness often called specific modulus is defined as the ratio of elastic modulus to mass density of a material. Rafiee and Moghadam [35] reported the density of epoxy resin as 890 kg/m^3 which is the corresponding value of the pure epoxy simulated in this study. Same value is used for the determination of specific stiffness of both epoxy and epoxy/SWNT composite. The density of composite is estimated by multiplying volume fractions of both SWNT and epoxy resin with their respective mass densities. Density of SWNT is taken as 1300 kg/m^3 (1.3 g/cm^3) [2].

Table 4.5 Characteristics of epoxy resin and its composite

Parameter	Pure Epoxy	Composite
Young's Modulus (GPa)	10	54.47
Density (kg/m^3)	890	910.5
Specific Stiffness ($MPa/kg/m^3$)	11.24	59.82

As demonstrated in Table 4.5, specific stiffness of pure epoxy is found to be 11.24 $MPa/kg/m^3$ while composite with 5% armchair (10,10) SWNT by volume in the polymer matrix possesses a value of 59.82 $MPa/kg/m^3$. For a specific application with given strength and fixed volume, epoxy/SWNT composite provides an opportunity of reducing material use by 5 times compared to that of pure epoxy resin. If this composite is to be used in automobiles or aerospace sectors, not only material savings but also improved fuel efficiency and better mileage will be achieved as demonstrated in a case study presented by Donnell et al. [9]. This comparison is crude and need to be refined further by a detailed study on the impact analysis of CNTRPs improving the performance of its potential applications under appropriate simulation environments and considerations.

Chapter 5

CONCLUSIONS AND FUTURE WORK

5.1. Conclusions

Carbon nanotube reinforced polymer composites (CNTRPs) possess higher material strength which can provide major breakthroughs to the applications where low weight and high stiffness is required. Reinforcement of carbon nanotubes into the polymer matrix is still not a mature technology due to several reasons discussed in the introduction and literature review. Therefore, assessment of mechanical properties of these nanocomposites will not only add value to the sustainable development but also lead towards convergence of the values of their mechanical material properties towards a focal range, which currently seems considerably scattered. This research specifically investigates the effects of chirality and size of single-walled carbon nanotubes (SWNTs) on the mechanical properties of both SWNTs and carbon nanotube reinforced epoxy composite.

First, a novel 3D beam element is developed based on equivalent-continuum mechanics approach and used for replacing C-C chemical bond for modelling SWNTs. With the help of aforementioned beam elements with circular cross-section, FE models are generated for a range of SWNTs. The effects of diameter and chirality on the mechanical properties of SWNTs are studied. It can be concluded that the nanotube diameter affects the mechanical properties of SWNTs to a great extent especially for small diameters and start approaching towards similar values for the large diameter nanotubes. As far as chiral effects are concerned, armchair SWNTs possess higher Young's moduli and Poisson's ratios as compared to the chiral and zigzag configurations, while chiral configurations have greater values of shear moduli than armchair and zigzag configurations. Chiral effects over shear strain are insignificant. The results are comparable to the similar studies added to the literature previously. This proposed approach for modelling SWNTs is capable of providing a valuable tool for determining the mechanical properties of CNTRPs as these are the contemporary materials having potential to replace existing composites and build new markets offering superior properties.

A good agreement between obtained results for SWNTs and published values in the literature establishes confidence in correct modelling process for CNTRPs. For the CNTRP models, the aforementioned SWNTs are embedded into the polymer resin which is selected to be epoxy as it has sustainable aspects associated with it. The volume fraction of SWNTs in polymer resin is chosen as 5% while the diameter for interface region between the two phases is picked as twice. For modelling interface regions, two approaches named non-bonded interactions and perfect bonding model are used and compared against each other. The comparison is novel itself since the first approach is developed recently and has not been sufficiently studied. Second approach is employed for evaluating the effects of chirality and size of SWNTs on the mechanical properties of CNTRPs which does not appear to be reported earlier. It is concluded that the SWNT diameter affects the mechanical properties of CNTRPs signified by their respective RVEs to a large extent especially for small diameters and converge to almost similar values for nanotubes with large diameters. On average, armchair RVEs possess higher values of Young's moduli and Poisson's ratios followed by chiral and then zigzag RVEs. Although there are not many studies available in literature on this particular subject, the results of this research are comparable to few of those found in literature. The results for Young's moduli are also in good agreement with those calculated by a theoretical relation known as continuum rule of mixtures.

On the whole, it can be understood that the selection of nanotube configuration to be reinforced into the polymer matrices depends upon the application. Armchair reinforcements are suitable for applications where higher strengths are required while zigzag can serve well when the requirement for strength is relatively less. In order to quantify the structural mass reduction by using these CNTRPs for a particular application, specific strength is calculated for both pure epoxy resin and its composite. Results show that the structural mass can be reduced 5 times to that of epoxy resin if its nanocomposite is used in its potential applications where the strength and volume requirements are fixed such as parts for automobiles and aircrafts. This mass reduction will ultimately lead towards better mileage, fuel savings and reduction in carbon emissions.

5.2. Future Work

In this research only those mechanical properties for the whole RVE are investigated which are assigned separately to each phase including SWNT, interface and polymer matrix. For the

continuation and future work, the developed RVE models can be used to assess other mechanical properties which are applications specific such as flexural strength, ultimate tensile/rupture strength, yield strength etc. The continuum rule of mixtures suggests that greater volume fractions of SWNTs into the polymer matrix eventually increase the elastic moduli of the resulting nanocomposites. Therefore, a comparison can be made in the future to assess the effect on not only Young's moduli but on other mechanical properties of CNTRPs as well by varying SWNT volume fractions. Apart from mechanical properties, the results can directly be applied to models capable of running real time simulations for specific applications to study the performance levels in detail.

Furthermore, one can apply the same modelling techniques and analysis with different polymer resins following a structural pattern like SWNT reinforcement into polyethylene (PE) followed by reinforcement into polypropylene (PP) with an increase carbon atom into its primary chain and so on. Finally, beside all of the aforementioned areas, one can follow the same methodology developed in this study to model RVEs in a way where SWNT are not aligned to the orientation of its surrounding matrix. This will result into less efficient load transfer from the host polymer to the reinforced SWNT which is more likely the case in actual. This modelling approach seems never applied before and can draw more realistic conclusions but at the same time, it is highly challenging and need to be modelled in a more sophisticated manner.

REFERENCES

[1] V. P. Sharma, V. Agarwal, S. Umar, and A. K. Singh, "Polymer Composites Sustainability: Environmental Perspective, Future Trends and Minimization of Health Risk," presented at the 2nd International Conference on Environmental Science and Development IPCBEE, 2011, Singapore, 2011, vol. 4, pp. 259–161.

[2] O. Breuer and U. Sundararaj, "Big returns from small fibers: A review of polymer/carbon nanotube composites," *Polymer Composites*, vol. 25, no. 6, pp. 630–645, Dec. 2004.

[3] F. Hussain, M. Hojjati, M. Okamoto, and R. E. Gorga, "Review article: Polymer-matrix Nanocomposites, Processing, Manufacturing, and Application: An Overview," *Journal of Composite Materials*, vol. 40, no. 17, pp. 1511–1575, Sep. 2006.

[4] X. Lu and Z. Hu, "Mechanical property evaluation of single-walled carbon nanotubes by finite element modeling," *Composites Part B: Engineering*, vol. 43, no. 4, pp. 1902–1913, Jun. 2012.

[5] R. Rafiee and R. M. Moghadam, "On the modeling of carbon nanotubes: A critical review," *Composites Part B: Engineering*, vol. 56, pp. 435–449, Jan. 2014.

[6] Y. W. Mai, Yu, and M. Institute of Materials, *Polymer nanocomposites*. Boca Raton, FL; Cambridge, England: CRC Press ; Woodhead, 2006.

[7] G. M. Odegard, T. S. Gates, K. E. Wise, C. Park, and E. J. Siochi, "Constitutive modeling of nanotube–reinforced polymer composites," *Composites Science and Technology*, vol. 63, no. 11, pp. 1671–1687, Aug. 2003.

[8] P.-C. Ma and J.-K. Kim, *Carbon Nanotubes for Polymer Reinforcement*. CRC Press, 2011.

[9] S. E. O'Donnell, K. R. Sprong, and B. M. Haltli, "Potential Impact of Carbon Nanotube Reinforced Polymer Composite on Commercial Aircraft Performance and Economics," *mitre.org*, Jan-2005. [Online]. Available: http://www.mitre.org/publications/technical-papers/potential-impact-of-carbon-nanotube-reinforced-polymer-composite-on-commercial-aircraft-performance-and-economics. [Accessed: 03-Oct-2013].

[10] J. C. Salamone, *Polymeric Materials Encyclopedia, Twelve Volume Set*. CRC Press, 1996.

[11] T. P. Chua, M. Mariatti, A. Azizan, and A. A. Rashid, "Effects of surface-functionalized multi-walled carbon nanotubes on the properties of poly(dimethyl siloxane) nanocomposites," *Composites Science and Technology*, vol. 70, no. 4, pp. 671–677, Apr. 2010.

[12] X.-L. Xie, Y.-W. Mai, and X.-P. Zhou, "Dispersion and alignment of carbon nanotubes in polymer matrix: A review," *Materials Science and Engineering: R: Reports*, vol. 49, no. 4, pp. 89–112, May 2005.

[13] J. Han, M. P. Anantram, R. L. Jaffe, J. Kong, and H. Dai, "Observation and modeling of single-wall carbon nanotube bend junctions," *Phys. Rev. B*, vol. 57, no. 23, pp. 14983–14989, Jun. 1998.

[14] A. R. Bhattacharyya, T. . Sreekumar, T. Liu, S. Kumar, L. M. Ericson, R. H. Hauge, and R. E. Smalley, "Crystallization and orientation studies in polypropylene/single wall carbon nanotube composite," *Polymer*, vol. 44, no. 8, pp. 2373–2377, Apr. 2003.

[15] S. S. Kin-tak Lau, "Failure mechanisms of carbon nanotube/epoxy composites pretreated in different temperature environments," *Carbon*, vol. 40, no. 15, pp. 2965–2968, 2002.

[16] Z. Jia, Z. Wang, C. Xu, J. Liang, B. Wei, D. Wu, and S. Zhu, "Study on poly(methyl methacrylate)/carbon nanotube composites," *Materials Science and Engineering: A*, vol. 271, no. 1–2, pp. 395–400, Nov. 1999.

[17] L. S. Schadler, S. C. Giannaris, and P. M. Ajayan, "Load transfer in carbon nanotube epoxy composites," *Applied Physics Letters*, vol. 73, no. 26, p. 3842, Dec. 1998.

[18] R. Haggenmueller, H. H. Gommans, A. G. Rinzler, J. E. Fischer, and K. I. Winey, "Aligned single-wall carbon nanotubes in composites by melt processing methods," *Chemical Physics Letters*, vol. 330, no. 3–4, pp. 219–225, Nov. 2000.

[19] M. Wong, M. Paramsothy, X. J. Xu, Y. Ren, S. Li, and K. Liao, "Physical interactions at carbon nanotube-polymer interface," *Polymer*, vol. 44, no. 25, pp. 7757–7764, Dec. 2003.

[20] D. Qian, E. C. Dickey, R. Andrews, and T. Rantell, "Load transfer and deformation mechanisms in carbon nanotube-polystyrene composites," *Applied Physics Letters*, vol. 76, no. 20, p. 2868, May 2000.

[21] Liu, I. Y. Phang, L. Shen, S. Y. Chow, and W.-D. Zhang, "Morphology and Mechanical Properties of Multiwalled Carbon Nanotubes Reinforced Nylon-6 Composites," *Macromolecules*, vol. 37, no. 19, pp. 7214–7222, Sep. 2004.

[22] S. Ganguli, H. Aglan, and D. Dean, "Microstructural Origin of Strength and Toughness of Epoxy Nanocomposites," *Journal of Elastomers and Plastics*, vol. 37, no. 1, pp. 19–35, Jan. 2005.

[23] J. R. Xiao, B. A. Gama, and J. W. Gillespie Jr., "An analytical molecular structural mechanics model for the mechanical properties of carbon nanotubes," *International Journal of Solids and Structures*, vol. 42, no. 11–12, pp. 3075–3092, Jun. 2005.

[24] J. Gollub, "Continuum Mechanics in Physics Education," *Physics Today*, vol. 56, pp. 10–11, Dec. 2003.

[25] B. I. Yakobson, C. J. Brabec, and J. Bernholc, "Nanomechanics of Carbon Tubes: Instabilities beyond Linear Response," *Phys. Rev. Lett.*, vol. 76, no. 14, pp. 2511–2514, Apr. 1996.

[26] T. Natsuki and M. Endo, "Stress simulation of carbon nanotubes in tension and compression," *Carbon*, vol. 42, no. 11, pp. 2147–2151, 2004.

[27] A. Pantano, D. M. Parks, and M. C. Boyce, "Mechanics of deformation of single- and multi-wall carbon nanotubes," *Journal of the Mechanics and Physics of Solids*, vol. 52, no. 4, pp. 789–821, Apr. 2004.

[28] G. M. Odegard, T. S. Gates, L. M. Nicholson, and K. E. Wise, "Equivalent-continuum modeling of nano-structured materials," *Composites Science and Technology*, vol. 62, no. 14, pp. 1869–1880, Nov. 2002.

[29] M. Meo and M. Rossi, “Prediction of Young’s modulus of single wall carbon nanotubes by molecular-mechanics based finite element modelling,” *Composites Science and Technology*, vol. 66, no. 11–12, pp. 1597–1605, Sep. 2006.

[30] C. Li and T.-W. Chou, “A structural mechanics approach for the analysis of carbon nanotubes,” *International Journal of Solids and Structures*, vol. 40, no. 10, pp. 2487–2499, May 2003.

[31] K. I. Tserpes and P. Papanikos, “Finite element modeling of single-walled carbon nanotubes,” *Composites Part B: Engineering*, vol. 36, no. 5, pp. 468–477, Jul. 2005.

[32] B. Jalalahmadi and R. Naghdabadi, “Finite element modeling of single-walled carbon nanotubes with introducing a new wall thickness,” *J. Phys.: Conf. Ser.*, vol. 61, no. 1, p. 497, Mar. 2007.

[33] M. R. Ayatollahi, S. Shadlou, and M. M. Shokrieh, “Multiscale modeling for mechanical properties of carbon nanotube reinforced nanocomposites subjected to different types of loading,” *Composite Structures*, vol. 93, no. 9, pp. 2250–2259, Aug. 2011.

[34] R. Rafiee, A. Fereidoon, and M. Heidarhaei, “Influence of non-bonded interphase on crack driving force in carbon nanotube reinforced polymer,” *Computational Materials Science*, vol. 56, pp. 25–28, Apr. 2012.

[35] R. Rafiee and R. Maleki Moghadam, “Simulation of impact and post-impact behavior of carbon nanotube reinforced polymer using multi-scale finite element modeling,” *Computational Materials Science*, vol. 63, pp. 261–268, Oct. 2012.

[36] M. M. Shokrieh and R. Rafiee, “Prediction of mechanical properties of an embedded carbon nanotube in polymer matrix based on developing an equivalent long fiber,” *Mechanics Research Communications*, vol. 37, no. 2, pp. 235–240, Mar. 2010.

[37] F. Karimzadeh, S. Ziaei-Rad, and S. Adibi, “Modeling Considerations and Material Properties Evaluation in Analysis of Carbon Nano-Tubes Composite,” *Metall and Materi Trans B*, vol. 38, no. 4, pp. 695–705, Aug. 2007.

[38] H. Wan, F. Delale, and L. Shen, “Effect of CNT length and CNT-matrix interphase in carbon nanotube (CNT) reinforced composites,” *Mechanics Research Communications*, vol. 32, no. 5, pp. 481–489, Sep. 2005.

[39] A. H. Barber, S. R. Cohen, S. Kenig, and H. D. Wagner, “Interfacial fracture energy measurements for multi-walled carbon nanotubes pulled from a polymer matrix,” *Composites Science and Technology*, vol. 64, no. 15, pp. 2283–2289, Nov. 2004.

[40] R. Qiao and L. Catherine Brinson, “Simulation of interphase percolation and gradients in polymer nanocomposites,” *Composites Science and Technology*, vol. 69, no. 3–4, pp. 491–499, Mar. 2009.

[41] F. Scarpa and S. Adhikari, “A mechanical equivalence for Poisson’s ratio and thickness of C–C bonds in single wall carbon nanotubes,” *J. Phys. D: Appl. Phys.*, vol. 41, no. 8, p. 085306, Apr. 2008.

[42] S. Timoshenko, *Theory of elasticity*, 2d ed. New York: McGraw-Hill, 1951.

[43] T. C. T. Ting and T. Chen, “Poisson’s ratio for anisotropic elastic materials can have no bounds,” *Q J Mechanics Appl Math*, vol. 58, no. 1, pp. 73–82, Feb. 2005.

[44] E. Hernandez, C. Goze, P. Bernier, and A. Rubio, “Elastic Properties of C and BxCyNz Composite Nanotubes,” *Physical Review Letters*, vol. 80, no. 20, pp. 4502–4505, May 1998.

[45] Y. Jin and F. G. Yuan, “Simulation of elastic properties of single-walled carbon nanotubes,” *Composites Science and Technology*, vol. 63, no. 11, pp. 1507–1515, Aug. 2003.

[46] C. Li and T.-W. Chou, “Elastic moduli of multi-walled carbon nanotubes and the effect of van der Waals forces,” *Composites Science and Technology*, vol. 63, no. 11, pp. 1517–1524, Aug. 2003.

[47] O. L. Blakslee, D. G. Proctor, E. J. Seldin, G. B. Spence, and T. Weng, “Elastic Constants of Compression-Annealed Pyrolytic Graphite,” *Journal of Applied Physics*, vol. 41, no. 8, pp. 3373–3382, Nov. 2003.

[48] B. WenXing, Z. ChangChun, and C. WanZhao, "Simulation of Young's modulus of single-walled carbon nanotubes by molecular dynamics," *Physica B: Condensed Matter*, vol. 352, no. 1–4, pp. 156–163, Oct. 2004.

[49] B. T. Kelly, *Physics of graphite*. London, Englewood, N.J: Applied Science, 1981.

[50] A. Krishnan, E. Dujardin, T. W. Ebbesen, P. N. Yianilos, and M. M. J. Treacy, "Young's modulus of single-walled nanotubes," *Phys. Rev. B*, vol. 58, no. 20, pp. 14013–14019, Nov. 1998.

[51] V. N. Popov, V. E. Van Doren, and M. Balkanski, "Elastic properties of single-walled carbon nanotubes," *Phys. Rev. B*, vol. 61, no. 4, pp. 3078–3084, Jan. 2000.

[52] A. F. Ávila and G. S. R. Lacerda, "Molecular mechanics applied to single-walled carbon nanotubes," *Materials Research*, vol. 11, no. 3, pp. 325–333, Sep. 2008.

[53] Z. Xin, Z. Jianjun, and O.-Y. Zhong-can, "Strain energy and Young's modulus of single-wall carbon nanotubes calculated from electronic energy-band theory," *Phys. Rev. B*, vol. 62, no. 20, pp. 13692–13696, Nov. 2000.

[54] Z. Tu and Z. Ou-Yang, "Single- and multi-walled carbon nanotubes viewed as elastic tubes with Young's moduli dependent on layer number," *Physical Review B*, vol. 65, no. 23, Jun. 2002.

[55] K. N. Kudin, G. E. Scuseria, and B. I. Yakobson, "C_{2}F, BN, and C nanoshell elasticity from ab initio computations," *Phys. Rev. B*, vol. 64, no. 23, p. 235406, Nov. 2001.

[56] X.-L. Gao and K. Li, "Finite deformation continuum model for single-walled carbon nanotubes," *International Journal of Solids and Structures*, vol. 40, no. 26, pp. 7329–7337, Dec. 2003.

[57] J. P. Lu, "Elastic Properties of Carbon Nanotubes and Nanoropes," *Phys. Rev. Lett.*, vol. 79, no. 7, pp. 1297–1300, Aug. 1997.

[58] F. Beer, J. J. Russell E., J. DeWolf, and D. Mazurek, *Mechanics of Materials*. McGraw-Hill Companies,Incorporated, 2008.

[59] C. Goze, L. Vaccarini, L. Henrard, P. Bernier, E. Hemandez, and A. Rubio, "Elastic and mechanical properties of carbon nanotubes," *Synthetic Metals*, vol. 103, no. 1–3, pp. 2500–2501, Jun. 1999.

[60] J. L. Bahr and J. M. Tour, "Covalent chemistry of single-wall carbon nanotubes," *J. Mater. Chem.*, vol. 12, no. 7, pp. 1952–1958, Jun. 2002.

[61] S. J. V. Frankland, A. Caglar, D. W. Brenner, and M. Griebel, "Molecular Simulation of the Influence of Chemical Cross-Links on the Shear Strength of Carbon Nanotube−Polymer Interfaces," *J. Phys. Chem. B*, vol. 106, no. 12, pp. 3046–3048, Mar. 2002.

[62] C. A. Cooper, S. R. Cohen, A. H. Barber, and H. D. Wagner, "Detachment of nanotubes from a polymer matrix," *Applied Physics Letters*, vol. 81, no. 20, pp. 3873–3875, Nov. 2002.

[63] Y. D. Kuang and X. Q. He, "Young's moduli of functionalized single-wall carbon nanotubes under tensile loading," *Composites Science and Technology*, vol. 69, no. 2, pp. 169–175, Feb. 2009.

[64] V. Lordi and N. Yao, "Molecular mechanics of binding in carbon-nanotube–polymer composites," *Journal of Materials Research*, vol. 15, no. 12, pp. 2770–2779, 2000.

[65] J. M. Wernik and S. A. Meguid, "Multiscale modeling of the nonlinear response of nano-reinforced polymers," *Acta Mech*, vol. 217, no. 1–2, pp. 1–16, Feb. 2011.

[66] A. L. Kalamkarov, A. V. Georgiades, S. K. Rokkam, V. P. Veedu, and M. N. Ghasemi-Nejhad, "Analytical and numerical techniques to predict carbon nanotubes properties," *International Journal of Solids and Structures*, vol. 43, no. 22–23, pp. 6832–6854, Nov. 2006.

[67] S. S. Batsanov, "Van der Waals Radii of Elements," *Inorganic Materials*, vol. 37, no. 9, pp. 871–885, Sep. 2001.

[68] J. N. Coleman, U. Khan, W. J. Blau, and Y. K. Gun'ko, "Small but strong: A review of the mechanical properties of carbon nanotube–polymer composites," *Carbon*, vol. 44, no. 9, pp. 1624–1652, Aug. 2006.

[69] H. L. Cox, “The elasticity and strength of paper and other fibrous materials,” *Br. J. Appl. Phys.*, vol. 3, no. 3, p. 72, Mar. 1952.

APPENDIX A

CHARACTERISTICS OF SWNT AND RVE FE MODELS

Table A.1 Characteristics of SWNT FE models

SWCNTS	Diameter (nm)	Chirality (deg)	Length (nm)	Nodes	Elements
Armchair					
(3,3)	0.407	30	12.298	600	894
(6,6)	0.814	30	12.052	1176	1752
(10,10)	1.356	30	12.052	1960	2920
(12,12)	1.627	30	12.052	2352	3504
(15,15)	2.034	30	12.052	2940	4380
Zigzag					
(6,0)	0.47	0	12.354	696	1032
(11,0)	0.861	0	11.928	1232	1837
(15,0)	1.174	0	12.354	1740	2595
(20,0)	1.566	0	12.354	2320	3440
(25,0)	1.957	0	12.354	2900	4299
Chiral					
(4,2)	0.414	19.1	13.525	672	1000
(8,4)	0.829	19.1	12.398	1232	1836
(12,6)	1.243	19.1	12.398	1848	2748
(16,8)	1.657	19.1	12.398	2464	3672
(20,10)	2.071	19.1	12.398	3080	4590

Table A.2 Characteristics of RVE FE models

Reinforced SWNT	SWNT Radius (nm)	Chirality (deg)	Interface Radius (nm)	RVE Radius (nm)	Length (nm)	Nodes	Elements
Armchair							
(3,3)	0.204	30	0.407	1.664	7.377	6820	6000
(6,6)	0.407	30	0.814	2.365	7.377	8060	7200
(10,10)	0.678	30	1.356	3.079	7.377	9920	9000
(12,12)	0.814	30	1.627	3.388	7.377	10540	9600
Zigzag							
(6,0)	0.235	0	0.470	1.789	7.377	7440	6600
(11,0)	0.431	0	0.861	2.434	7.377	8680	7800
(15,0)	0.587	0	1.174	2.856	7.377	9300	8400
(20,0)	0.783	0	1.566	3.320	7.377	10540	9600
Chiral							
(4,2)	0.207	19.1	0.414	1.678	7.377	6820	6000
(8,4)	0.415	19.1	0.829	2.387	7.377	8060	7200
(12,6)	0.622	19.1	1.243	2.942	7.377	9920	9000
(16,8)	0.829	19.1	1.657	3.421	7.377	10540	9600

APPENDIX B

KEY SIMULATION RESULTS

Table B.1 SWNT Young's Modulus evaluation

SWNTs	Diameter (nm)	Chirality (deg)	Length (nm)	ΔL (nm)	F (nN)	Et (TPa.nm)	E (TPa)
Armchair							
(3,3)	0.407	30	12.298	0.100	3.108	0.299	0.879
(6,6)	0.814	30	12.052	0.100	6.359	0.300	0.881
(10,10)	1.356	30	12.052	0.100	10.612	0.300	0.883
(12,12)	1.627	30	12.052	0.100	12.738	0.300	0.883
(15,15)	2.034	30	12.052	0.100	15.930	0.300	0.884
					Average:	0.300	0.882
Zigzag							
(6,0)	0.470	0	12.354	0.100	3.292	0.275	0.810
(11,0)	0.861	0	11.928	0.100	6.675	0.294	0.866
(15,0)	1.174	0	12.354	0.100	8.904	0.298	0.877
(20,0)	1.566	0	12.354	0.100	11.940	0.300	0.882
(25,0)	1.957	0	12.354	0.100	14.952	0.300	0.884
					Average:	0.294	0.864
Chiral							
(4,2)	0.414	19.1	13.525	0.100	2.782	0.289	0.851
(8,4)	0.829	19.1	12.398	0.100	6.279	0.299	0.879
(12,6)	1.243	19.1	12.398	0.100	9.420	0.299	0.880
(16,8)	1.657	19.1	12.398	0.100	12.651	0.301	0.886
(20,10)	2.071	19.1	12.398	0.100	15.828	0.302	0.887
					Average:	0.298	0.877

Table B.2 SWNT shear modulus evaluation

SWNTs	Diameter (nm)	Chirality (deg)	Length (nm)	Thickness (nm)	Torsion (nN.nm)	J $(nm)^4$	Ø (rad)	G (TPa)
Armchair								
(3,3)	0.407	30	12.298	0.340	0.600	0.031	0.927	0.260
(6,6)	0.814	30	12.052	0.340	1.200	0.169	0.285	0.300
(10,10)	1.356	30	12.052	0.340	2.000	0.708	0.098	0.348
(12,12)	1.627	30	12.052	0.340	2.400	1.200	0.069	0.349
(15,15)	2.034	30	12.052	0.340	3.000	2.310	0.043	0.362
							Average:	0.324
Zigzag								
(6,0)	0.470	0	12.354	0.340	0.600	0.042	0.652	0.269
(11,0)	0.861	0	11.928	0.340	1.100	0.197	0.212	0.315
(15,0)	1.174	0	12.354	0.340	1.500	0.468	0.117	0.339
(20,0)	1.566	0	12.354	0.340	2.000	1.074	0.068	0.339
(25,0)	1.957	0	12.354	0.340	2.500	2.062	0.043	0.345
							Average:	0.321
Chiral								
(4,2)	0.414	19.1	13.525	0.340	0.600	0.032	0.891	0.287
(8,4)	0.829	19.1	12.398	0.340	1.200	0.178	0.262	0.319
(12,6)	1.243	19.1	12.398	0.340	1.800	0.551	0.117	0.345
(16,8)	1.657	19.1	12.398	0.340	2.400	1.266	0.065	0.362
(20,10)	2.071	19.1	12.398	0.340	3.000	2.436	0.042	0.362
							Average:	0.335

Table B.3 SWNT shear strain evaluation

SWNTs	Diameter (nm)	Chirality (deg)	Length (nm)	Thickness (nm)	Torsion (nN.nm)	Ø (rad)	γ
Armchair							
(3,3)	0.407	30	12.298	0.340	0.600	0.927	0.015
(6,6)	0.814	30	12.052	0.340	1.200	0.285	0.010
(10,10)	1.356	30	12.052	0.340	2.000	0.098	0.006
(12,12)	1.627	30	12.052	0.340	2.400	0.069	0.005
(15,15)	2.034	30	12.052	0.340	3.000	0.043	0.004
						Average:	0.008
Zigzag							
(6,0)	0.470	0	12.354	0.340	0.600	0.652	0.012
(11,0)	0.861	0	11.928	0.340	1.100	0.212	0.008
(15,0)	1.174	0	12.354	0.340	1.500	0.117	0.006
(20,0)	1.566	0	12.354	0.340	2.000	0.068	0.004
(25,0)	1.957	0	12.354	0.340	2.500	0.043	0.003
						Average:	0.007
Chiral							
(4,2)	0.414	19.1	13.525	0.340	0.600	0.891	0.014
(8,4)	0.829	19.1	12.398	0.340	1.200	0.262	0.009
(12,6)	1.243	19.1	12.398	0.340	1.800	0.117	0.006
(16,8)	1.657	19.1	12.398	0.340	2.400	0.065	0.004
(20,10)	2.071	19.1	12.398	0.340	3.000	0.042	0.004
						Average:	0.007

Table B.4 SWNT Poisson's ratio evaluation

SWNTs	Diameter (nm)	Chirality (deg)	Length (nm)	ΔL (nm)	Δd (nm)	ν
Armchair						
(3,3)	0.407	30	12.298	2.000	-0.030	0.457
(6,6)	0.814	30	12.052	2.000	-0.038	0.279
(10,10)	1.356	30	12.052	2.000	-0.057	0.254
(12,12)	1.627	30	12.052	2.000	-0.067	0.250
(15,15)	2.034	30	12.052	2.000	-0.082	0.244
					Average:	0.297
Zigzag						
(6,0)	0.470	0	12.354	2.000	-0.023	0.296
(11,0)	0.861	0	11.928	2.000	-0.035	0.245
(15,0)	1.174	0	12.354	2.000	-0.045	0.234
(20,0)	1.566	0	12.354	2.000	-0.058	0.229
(25,0)	1.957	0	12.354	2.000	-0.073	0.230
					Average:	0.247
Chiral						
(4,2)	0.414	19.1	13.525	2.000	-0.044	0.725
(8,4)	0.829	19.1	12.398	2.000	-0.037	0.276
(12,6)	1.243	19.1	12.398	2.000	-0.058	0.288
(16,8)	1.657	19.1	12.398	2.000	-0.062	0.233
(20,10)	2.071	19.1	12.398	2.000	-0.078	0.233
					Average:	0.351

Table B.5 RVE Young's Modulus evaluation

Reinforced SWNTs	RVE Area (nm^2)	Chirality (deg)	Length (nm)	ΔL (nm)	F (nN)	Stress (GPa)	Strain	E (GPa)
Armchair								
(3,3)	8.695	30	7.377	0.100	6.331	0.728	0.014	53.712
(6,6)	17.389	30	7.377	0.100	12.656	0.728	0.014	53.692
(10,10)	28.968	30	7.377	0.100	21.389	0.738	0.014	54.470
(12,12)	34.757	30	7.377	0.100	25.836	0.743	0.014	54.834
							Average:	54.177
Zigzag								
(6,0)	10.041	0	7.377	0.100	6.763	0.674	0.014	49.688
(11,0)	18.393	0	7.377	0.100	13.216	0.719	0.014	53.006
(15,0)	25.080	0	7.377	0.100	18.324	0.731	0.014	53.898
(20,0)	33.454	0	7.377	0.100	24.777	0.741	0.014	54.635
							Average:	52.807
Chiral								
(4,2)	8.844	19.1	7.377	0.100	6.189	0.700	0.014	51.619
(8,4)	17.710	19.1	7.377	0.100	12.881	0.727	0.014	53.657
(12,6)	26.554	19.1	7.377	0.100	19.539	0.736	0.014	54.282
(16,8)	35.398	19.1	7.377	0.100	26.384	0.745	0.014	54.983
							Average:	53.636

Table B.6 RVE Poisson's ratio evaluation

Reinforced SWNTs	RVE Area (nm^2)	Chirality (deg)	Length (nm)	ΔL (nm)	Δd (nm)	ν
Armchair						
(3,3)	8.695	30	7.377	2.000	-0.284	0.315
(6,6)	17.389	30	7.377	2.000	-0.370	0.289
(10,10)	28.968	30	7.377	2.000	-0.447	0.268
(12,12)	34.757	30	7.377	2.000	-0.475	0.259
					Average:	0.283
Zigzag						
(6,0)	10.041	0	7.377	2.000	-0.292	0.301
(11,0)	18.393	0	7.377	2.000	-0.374	0.284
(15,0)	25.080	0	7.377	2.000	-0.421	0.272
(20,0)	33.454	0	7.377	2.000	-0.464	0.258
					Average:	0.279
Chiral						
(4,2)	8.844	19.1	7.377	2.000	-0.276	0.303
(8,4)	17.710	19.1	7.377	2.000	-0.372	0.288
(12,6)	26.554	19.1	7.377	2.000	-0.440	0.276
(16,8)	35.398	19.1	7.377	2.000	-0.474	0.255
					Average:	0.281

APPENDIX C

SENSITIVITY ANALYSIS FOR RVE-2

Since Approach-2 i.e. perfect bonding model is based entirely on solid brick elements, therefore, it is essential to compute consistent response sensitivities of the representative volume element using the same approach. For this purpose, armchair (10,10) RVE-2 is employed to perform sensitivity analysis. Table C.1 shows the characteristics of RVE FE models and demonstrates the results computed for Young's moduli.

Table C.1 Variation of Young's modulus of armchair (10,10) RVE-2 by changing number of elements

No. of Elements	RVE Area (nm^2)	Length (nm)	ΔL (nm)	Force (nN)	E GPa
3600	28.968	7.377	0.100	21.404	54.507
4200	28.968	7.377	0.100	21.395	54.486
6000	28.968	7.377	0.100	21.391	54.473
9000	28.968	7.377	0.100	21.389	54.470
12000	28.968	7.377	0.100	21.389	54.469
15000	28.968	7.377	0.100	21.389	54.469

Figure C.1 illustrates the response sensitivities of model RVE by varying number of elements. It can be seen from the figure that after 9000 elements, the values for Young's modulus of RVE remains almost same i.e. 54.469 GPa. Therefore, the size of solid brick elements determined from the FE mesh with 9000 elements is taken as reference to develop all the remaining RVE models employing Approach 2.

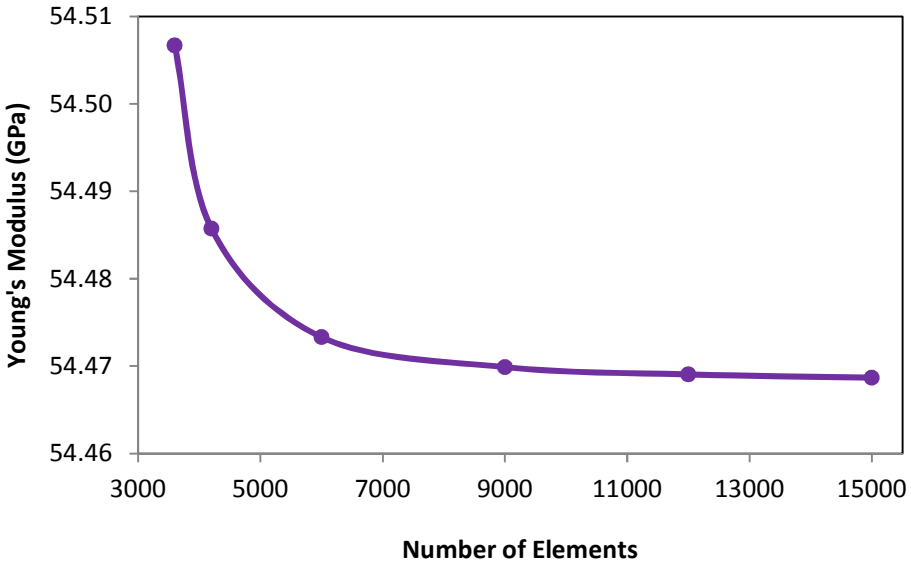

Figure C.1 Young's modulus response sensitivity for (10,10) RVE-2